Fast two-scale methods for Eikonal equations.

Adam Chacon and Alexander Vladimirsky[1]

Department of Mathematics and Center for Applied Mathematics
Cornell University, Ithaca, NY 14853

Abstract.
Fast Marching and Fast Sweeping are the two most commonly used methods for solving the Eikonal equation. Each of these methods performs best on a different set of problems. Fast Sweeping, for example, will outperform Fast Marching on problems where the characteristics are largely straight lines. Fast Marching, on the other hand, is usually more efficient than Fast Sweeping on problems where characteristics frequently change their directions and on domains with complicated geometry. In this paper we explore the possibility of combining the best features of both of these approaches, by using marching on a coarser scale and sweeping on a finer scale. We present three new hybrid methods based on this idea and illustrate their properties on several numerical examples with continuous and piecewise-constant speed functions in R^2.

1. Introduction. Static Eikonal PDEs arise in a surprisingly wide range of applications: from robotic path planning, to isotropic optimal control, to isotropic front propagation, to shape-from-shading computations; see [38] and references therein for a detailed description. As a result, efficient numerical methods for Eikonal PDEs are of interest to many practitioners and numerical analysts. In this paper we introduce two hybrid methods intended to blend and combine the best properties of the most popular current approaches (Fast Marching and Fast Sweeping).

These methods are built to solve the non-linear boundary value problem[2]

$$\begin{aligned} |\nabla u(\boldsymbol{x})| F(\boldsymbol{x}) = 1, &\text{ on } \Omega \subset R^2; \\ u(\boldsymbol{x}) = q(\boldsymbol{x}), &\text{ on } \partial\Omega. \end{aligned} \tag{1.1}$$

A discretized version of equation (1.1) is posed at every gridpoint, using upwind divided differences to approximate the partial derivatives of u. The exact form of this discretization is introduced in section 2; here we simply note that these discretized equations form a system of M coupled non-linear equations (where M is the number of gridpoints) and that the key challenge addressed by many "fast" methods is the need to solve this system efficiently. Of course, an iterative approach is certainly a possibility, but its most straightforward and naive implementation typically leads to $O(M^2)$ algorithmic complexity for Eikonal PDE (and potentially much worse for its anisotropic generalizations). This is in contrast to the "fast" methods, whose worst-case computational complexity is $O(M)$ or $O(M \log M)$.

Interestingly, most fast Eikonal-solvers currently in use are directly related to the fast algorithms developed much earlier to find the shortest paths in directed graphs with non-negative edge-lengths; see, e.g., [1], [8, 9]. Two such algorithmic families are particularly prominent: the *label-setting methods*, which have the optimal worst-case asymptotic computational complexity, and the *label-correcting methods*, whose worst-case asymptotic complexity is not as good, but the practical performance is at times even better than that of label-setting. We provide a basic overview of both families in section 1.1. The prior fast Eikonal-solvers based on label-setting and label-correcting are reviewed in sections 2.1 and 2.2-2.3 respectively.

The most popular methods from these two categories (Fast Marching and Fast Sweeping) have been shown to be efficient on a wide range of Eikonal equations. However, each of these methods has its own preferred class of problems, on which it significantly outperforms the other. Despite experimental comparisons already conducted in [23] and [22], the exact delineation of a preferred

[1] This research is supported in part by the National Science Foundation grants DMS-0514487 and DMS-1016150. The first author's research is also supported by Alfred P. Sloan Foundation Graduate Fellowship.
This manuscript is an extended version of the paper submitted for publication in SIAM J. on Scientific Computing. In the journal version, subsections 4.4 and 4.5 and parts of section 3 were omitted due to space limitations.

[2] For simplicity, we will restrict our exposition to first-order accurate discretizations of these problems on Cartesian grids in R^2, although generalizations to higher dimensional domains are straightforward and similar approaches are applicable to higher-order accurate discretizations on unstructured meshes in R^n and on manifolds.

problem-set for each method is still a matter of debate. Fast Sweeping (reviewed in section 2.1) is usually more efficient on problems with constant characteristic directions. But for general functions $F(\boldsymbol{x})$, its computational cost is clearly impacted by the frequency and magnitude of directional changes of characteristic curves. Fast Marching (reviewed in section 2.1) is generally more efficient on domains with complicated geometry and on problems with characteristic directions frequently changing. Its causal algorithmic structure results in a provably converged solution on explicitly determined parts of the computational domain even before the method terminates – a very useful feature in many applications. Moreover, its efficiency is much more "robust"; i.e., its computational cost is much less affected by any changes in functions F and q or the grid orientation. But as a result, the Fast Marching also is not any faster in the simplest cases where F is constant on a convex domain and all characteristics are straight lines – the exact scenario where the Fast Sweeping is at its most efficient.

The fundamental idea underlying our hybrid two-scale methods is to take advantage of the best features of both marching and sweeping. Suppose the domain is split in a moderate number of cells such that F is almost-constant on each of them. (Such cell splitting is possible for any piecewise-smooth F.) On the top scale, a version of Fast Marching can be used on a coarse grid (with each gridpoint representing a cell of the fine grid). Once the ordering of coarse gridpoints is established, the Fast Sweeping is applied to individual cells of the fine grid in the same order. This is the basis of our Fast Marching-Sweeping Method (FMSM) described in section 3.1.

Unfortunately, the coarse grid ordering captures the information flow through the fine grid cells only approximately: a coarse gridpoint $\boldsymbol{y}_i$ might be "accepted" by Fast Marching before another coarse gridpoint $\boldsymbol{y}_j$, even if on the fine grid the characteristics cross both from cell i to cell j and from cell j to cell i. The "one-pass" nature of Fast Marching prevents FMSM from acting on such interdependencies between different cells even if they are revealed during the application of Fast Sweeping to these cells. To remedy this, we introduce the Heap-Cell Method (HCM) described in section 3.2. The idea is to allow multiple passes through fine grid cells sorted by the representative "cell-values" and updated as a result of cell-level fast sweeping. We also describe its heuristic version, the Fast Heap-Cell Method (FHCM), where the number of cell-level sweeps is determined based on the cell-boundary data.

Similarly to Fast Marching and Fast Sweeping, our HCM provably converges to the exact solution of the discretized equations on the fine scale. In contrast, the even faster FHCM and FMSM usually introduce additional errors. But based on our extensive numerical experiments (section 4), these additional errors are small compared to the errors already present due to discretization. The key advantage of all three new methods is their computational efficiency – with properly chosen cell sizes, we can significantly outperform both Fast Sweeping and Fast Marching on examples difficult for those methods, while matching their performance on the examples which are the easiest for each of them. We conclude by discussing the current limitations of our approach and several directions for future work in section 5.

1.1. Fast algorithms for paths on graphs.

We provide a brief review of common fast methods for the classical shortest/cheapest path problems on graphs. Our exposition follows [8] and [9], but with modifications needed to emphasize the parallels with the numerical methods in sections 2 and 3.

Consider a directed graph with nodes $X = \{\boldsymbol{x}_1, ..., \boldsymbol{x}_M\}$. Let $N(\boldsymbol{x}_i)$ be the set of nodes to which $\boldsymbol{x_i}$ is connected. We will assume that $\kappa \ll M$ is an upper bound on outdegrees; i.e., $|N(\boldsymbol{x}_i)| \leq \kappa$. We also suppose that all arc-costs $C_{ij} = C(\boldsymbol{x}_i, \boldsymbol{x}_j)$ are positive and use $C_{ij} = +\infty$ whenever $\boldsymbol{x}_j \notin N(\boldsymbol{x}_i)$. Every path terminates upon reaching the specified exit set $Q \subset X$, with an additional exit-cost $q_i = q(\boldsymbol{x}_i)$ for each $\boldsymbol{x}_i \in Q$. Given any starting node $\boldsymbol{x}_i \in X$, the goal is to find the cheapest path to the exit starting from $\boldsymbol{x}_i$. The *value function* $U_i = U(\boldsymbol{x}_i)$ is defined to be the optimal path-cost (minimized over all paths starting from $\boldsymbol{x}_i$). If there exists no path from $\boldsymbol{x}_i$ to Q, then $U_i = +\infty$, but for simplicity we will henceforth assume that Q is reachable from each $\boldsymbol{x}_i$ and all U_i's are finite.

The optimality principle states that the "tail" of every optimal path is also optimal; hence,

$$U_i = \min_{\boldsymbol{x}_j \in N(\boldsymbol{x}_i)} \{C_{ij} + U_j\}, \qquad \text{for } \forall \boldsymbol{x}_i \in X \backslash Q;$$
$$U_i = q_i, \qquad \text{for } \forall \boldsymbol{x}_i \in Q. \tag{1.2}$$

This is a coupled system of M non-linear equations, but it possesses a nice "causal" property: if $\boldsymbol{x}_j \in N(\boldsymbol{x}_i)$ is the minimizer, then $U_i > U_j$.

In principle, this system could be solved by "value iterations"; this approach is unnecessarily expensive (and is usually reserved for harder *stochastic* shortest path problems), but we describe it here for methodological reasons, to emphasize the parallels with "fast iterative" numerical methods for Eikonal PDEs. An operator T is defined on $\boldsymbol{R}^M$ component-wise by applying the right hand side of equation (1.2). Clearly, $U = \begin{bmatrix} U_1 \\ \vdots \\ U_M \end{bmatrix}$ is a fixed point of T and one can, in principle, recover U by *value iterations*:

$$W^{k+1} := T\,W^k \qquad \text{starting from any initial guess } W^0 \in \boldsymbol{R}^M. \tag{1.3}$$

Due to the causality of system (1.2), value iterations will converge to U regardless of W^0 after at most M iterations, resulting in $O(M^2)$ computational cost. (It is easy to show by induction that $W_i^k = U_i$ for every $\boldsymbol{x}_i$ from which there exists an optimal path with at most k transitions.) A Gauss-Seidel relaxation of this iterative process is a simple practical modification, where the entries of W^{k+1} are computed sequentially and the new values are used as soon as they become available: $W_i^{k+1} = T_i(W_1^{k+1}, \ldots, W_{i-1}^{k+1}, W_i^k, \ldots, W_M^k)$. The number of iterations required to converge will now heavily depend on the ordering of the nodes (though M is still the upper bound). We note that, again due to causality of (1.2), if the ordering is such that $U_i > U_j \implies i > j$, then only one full iteration will be required (i.e., $W^1 = U$ regardless of W^0). Of course, U is not known in advance and thus such a causal ordering is usually not available a priori (except in acyclic graphs). If several different node orderings are somehow known to capture likely dependency chains among the nodes, then a reasonable approach would be to perform Gauss-Seidel iterations alternating through that list of preferred orderings – this might potentially result in a substantial reduction in the number of needed iterations. In section 2.2 we explain how such preferred orderings arise from the geometric structure of PDE discretizations, but no such information is typically available in problems on graphs. As a result, instead of alternating through a list of predetermined orderings, efficient methods on graphs are based on finding advantageous orderings of nodes *dynamically.* This is the basis for *label-correcting* and *label-setting* methods.

A generic label-correcting method is summarized below in algorithm 1. It is easy to prove that this algorithm always terminates and that upon its termination $V = U$; e.g., see [8]. Many different label-correcting methods are obtained by using different choices on how to add the nodes to the list L and which node to remove (in the first line inside the while loop). If L is implemented as a queue, the node is typically removed from the top of L. Always adding the nodes at the bottom of L yields the *Bellman-Ford method* [6]. (This results in a first-in/first-out policy for processing the queue.) Always adding nodes at the top of L produces the *depth-first-search* method, with the intention of minimizing the memory footprint of L. Adding nodes at the top if they have already been in L before, while adding the "first-timers" at the bottom yields *D'Esopo-Pape method* [33]. Another interesting version is the so called *small-labels-first* (SLF) method [7], where the node is added at the top only if its value is smaller than that of the current top node and at the bottom otherwise. Another variation is *large-labels-last* (LLL) method [10], where the top node is removed only if its value is smaller than the current average of the queue; otherwise it's simply moved to the bottom of the queue instead. Yet another popular approach is called *thresholding method*, where L is split into two queues, nodes are removed from the first of them only and added to the first or the second queue depending on whether the labels are smaller than some (dynamically changing) threshold value [20]. We emphasize that the convergence is similarly obtained for all of these methods, their worst-case asymptotic complexity is $O(M^2)$, but their comparative efficiency for specific problems can be dramatically different.

Algorithm 1 Generic Label-Correcting pseudocode.

```
1: Initialization:
2: for each node $\boldsymbol{x}_i$ do
3:     if $\boldsymbol{x}_i \in Q$ then
4:         $V_i \leftarrow q_i$
5:     else
6:         if $N(\boldsymbol{x}_i) \bigcap Q \neq \emptyset$ then
7:             $V_i \leftarrow \min\limits_{\boldsymbol{x}_j \in N(\boldsymbol{x}_i) \bigcap Q} \{C_{ij} + q_j\}$
8:             add $\boldsymbol{x}_i$ to the list $L$
9:         else
10:            $V_i \leftarrow \infty$
11:        end if
12:    end if
13: end for
14:
15: Main Loop:
16: while $L$ is nonempty do
17:     Remove a node $\boldsymbol{x}_j$ from the list $L$
18:     for each $\boldsymbol{x}_i \notin Q$ such that $\boldsymbol{x}_j \in N(\boldsymbol{x}_i)$ and $V_j < V_i$ do
19:         $\widetilde{V} \leftarrow C_{ij} + V_j$
20:         if $\widetilde{V} < V_i$ then
21:             $V_i \leftarrow \widetilde{V}$
22:             if $\boldsymbol{x}_i \notin L$ then
23:                 add $\boldsymbol{x}_i$ to the list $L$
24:             end if
25:         end if
26:     end for
27: end while
```

Label-setting algorithms can be viewed as a subclass of the above with an additional property: nodes removed from L never need to be re-added later. Dijkstra's classical method [18] is the most popular in this category and is based on always removing the node with the smallest label of those currently in L. (The fact that this results in no re-entries into the list is yet another consequence of the causality; the inductive proof is simple; e.g., see [8].) The need to find the smallest label entails additional computational costs. A common implementation of L using heap-sort data structures will result in $O(M \log M)$ overall asymptotic complexity of the method on sparsely connected graphs (i.e., provided $\kappa \ll M$). Another version, due to Dial [17], implements L as a list of "buckets", so that all nodes in the current smallest bucket can be safely removed simultaneously, resulting in the overall asymptotic complexity of $O(M)$. The width of each bucket is usually set to be $\delta = \min_{i,j} C_{ij}$ to ensure that the nodes in the same bucket could not influence or update each other even if they were removed sequentially.

We note that several label-correcting methods were designed to mimic the "no-re-entry" property of label-setting, but without using expensive data structures. (E.g., compare SLF/LLL to Dijkstra's and thresholding to Dial's.) Despite the lower asymptotic complexity of label-setting methods, label-correcting algorithms can be more efficient on many problems. Which types of graphs favor which of these algorithms remains largely a matter of debate. We refer readers to [8, 9] and references therein for additional details and asynchronous (parallelizable) versions of label-correcting algorithms.

2. Eikonal PDE, upwind discretization & prior fast methods. Static Hamilton-Jacobi equations frequently arise in exit-time optimal control problems. The Eikonal PDE (1.1) describes an important subset: isotropic time-optimal control problems. The goal is to drive a system starting from a point $\boldsymbol{x} \in \Omega$ to exit the domain as quickly as possible. In this setting, $F : \Omega \to \boldsymbol{R}_+$ is the local speed of motion, and $q : \partial\Omega \to \boldsymbol{R}$ is the exit-time penalty charged at the boundary. We note that more general control problems (with an exit-set $Q \subset \partial\Omega$ and trajectories constrained to remain inside Ω until reaching Q) can be treated similarly by setting $q = +\infty$ on $\partial\Omega\backslash Q$.

The *value function* $u(\boldsymbol{x})$ is defined to be the minimum time-to-exit starting from $\boldsymbol{x}$ and a formal argument shows that u should satisfy the equation (1.1). Moreover, characteristics of this PDE, coinciding with the gradient lines of u, provide the optimal trajectories for moving through the domain. Unfortunately, the equation (1.1) usually does not have a classical (smooth) solution on the entire domain, while weak solutions are not unique. Additional test conditions are used to select among them the unique *viscosity solution*, which coincides with the value function of the original control problem [14, 13]. A detailed treatment of general optimal control problems in the framework of viscosity solutions can be found in [4].

Many discretization approaches for the Eikonal equation have been extensively studied including first-order and higher-order Eulerian discretizations on grids and meshes in $\boldsymbol{R}^n$ and on manifolds [36, 37, 28, 40], semi-Lagrangian discretizations [19, 21], and the related approximations with controlled Markov chains [29, 12]. For the purposes of this paper, we will focus on the simplest first-order upwind discretization on a uniform Cartesian grid X (with gridsize h) on $\overline{\Omega} \subset \boldsymbol{R}^2$. To simplify the description of algorithms, we will further assume that both $\partial\Omega$ and Q are naturally discretized on the grid X. Our exposition here closely follows [39, 38].

To introduce the notation, we will refer to gridpoints $\boldsymbol{x}_{ij} = (x_i, y_j)$, value function approximations $U_{ij} = U(\boldsymbol{x}_{ij}) \approx u(\boldsymbol{x}_{ij})$, and the speed $F_{ij} = F(\boldsymbol{x}_{ij})$. A popular first-order accurate discretization of (1.1) is obtained by using upwind finite-differences to approximate partial derivatives:

$$\left(\max\left(D^{-x}_{ij}U,\, -D^{+x}_{ij}U,\, 0\right)\right)^2 \;+\; \left(\max\left(D^{-y}_{ij}U,\, -D^{+y}_{ij}U,\, 0\right)\right)^2 \;=\; \frac{1}{F^2_{ij}}, \tag{2.1}$$

$$\text{where} \qquad u_x(x_i, y_j) \approx D^{\pm x}_{ij}U = \frac{U_{i\pm1,j} - U_{i,j}}{\pm h}; \qquad u_y(x_i, y_j) \approx D^{\pm y}_{ij}U = \frac{U_{i,j\pm1} - U_{i,j}}{\pm h}.$$

If the values at four surrounding nodes are known, this equation can be solved to recover U_{ij}. This is best accomplished by computing updates from individual quadrants as follows. Focusing on a single node $\boldsymbol{x}_{ij}$, we will simplify the notation by using $U = U_{ij}$, $F = F_{ij}$, and $\{U_E, U_N, U_W, U_S\}$ for the values at its four neighbor nodes.

First, suppose that $\max\left(D^{-x}_{ij}U,\, -D^{+x}_{ij}U,\, 0\right) = 0$ and $\max\left(D^{-y}_{ij}U,\, -D^{+y}_{ij}U,\, 0\right) = -D^{+y}_{ij}U$. This implies that $U \geq U_N$ and the resulting equation yields

$$U = h/F + U_N. \tag{2.2}$$

To compute "the update from the first quadrant", we now suppose that
$\max\left(D^{-x}_{ij}U,\, -D^{+x}_{ij}U,\, 0\right) = -D^{+x}_{ij}U$ and $\max\left(D^{-y}_{ij}U,\, -D^{+y}_{ij}U,\, 0\right) = -D^{+y}_{ij}U$.
This implies that $U \geq U_N$ and $U \geq U_E$. The resulting quadratic equation is

$$\left(\frac{U - U_E}{h}\right)^2 + \left(\frac{U - U_N}{h}\right)^2 = \frac{1}{F^2}. \tag{2.3}$$

We define "the update from the first quadrant" U^{NE} to be the root of the above quadratic satisfying $U \geq \max(U_N, U_E)$. If no such root is available, we use the smallest of the "one-sided" updates, similar to the previous case; i.e., $U^{NE} = h/F + \min(U_N, U_E)$. If we similarly define the updates from the remaining three quadrants, it is easy to show that $U = \min(U^{NE}, U^{NW}, U^{SW}, U^{SE})$ satisfies the original equation (2.1).

Remark 2.1. It is also easy to verify that this discretization is
- *consistent*, i.e., suppose both sides of (2.1) are multiplied by h^2; if the true solution $u(\boldsymbol{x})$ is smooth, it satisfies the resulting discretized equation up to $O(h^2)$;
- *monotone*, i.e., U is a non-decreasing function of each of its neighboring values;
- *causal*, i.e., U depends only on the neighboring values smaller than itself [37, 38].

The consistency and monotonicity can be used to prove the convergence to the viscosity solution $u(\boldsymbol{x})$; see [5]. However, since (2.1) has to hold at every gridpoint $\boldsymbol{x}_{ij} \in X\backslash Q$, this discretization results in a system of M coupled non-linear equations, where M is the number of gridpoints in the interior of Ω. In principle, this system can be solved iteratively (similarly to the "value iterations" process described in (1.3)) with or without Gauss-Seidel relaxation, but a naive implementation of this iterative algorithm would be unnecessarily expensive, since it does not take advantage of the causal properties of the discretization. Several competing approaches for solving the discretized system efficiently are reviewed in the following subsections.

2.1. Label-setting methods for the Eikonal. The causality property observed above is the basis of Dijkstra-like methods for the Eikonal PDE. The first such method was introduced by Tsitsiklis for isotropic control problems using first-order semi-Lagrangian discretizations on uniform Cartesian grids [45, 46]. The Fast Marching Method was introduced by Sethian [37] using first-order upwind-finite differences in the context of isotropic front propagation. A detailed discussion of similarities and differences of these approaches can be found in [42]. Sethian and collaborators have later extended the Fast Marching approach to higher-order discretizations on grids and meshes [39], more general anisotropic Hamilton-Jacobi-Bellman PDEs [41, 42], and quasi-variational inequalities [43]. Similar methods were also introduced for semi-Lagrangian discretizations [15]. The Fast Marching Method for the Eulerian discretization (2.1) is summarized below in Algorithm 2.

Algorithm 2 Fast Marching Method pseudocode.

```
1: Initialization:
2: for each gridpoint $\boldsymbol{x}_{ij} \in X$ do
3:     if $\boldsymbol{x}_{ij} \in Q$ then
4:         Label $\boldsymbol{x}_{ij}$ as Accepted and set $V_{ij} = q(\boldsymbol{x}_{ij})$.
5:     else
6:         Label $\boldsymbol{x}_{ij}$ as $Far$ and set $V_{ij} = \infty$.
7:     end if
8: end for
9: for each $Far$ neighbor $\boldsymbol{x}_{ij}$ of each Accepted node do
10:     Label $\boldsymbol{x}_{ij}$ as Considered and put $\boldsymbol{x}_{ij}$ onto the Considered List $L$.
11:     Compute a temporary value $\widetilde{V}_{ij}$ using the upwinding discretization.
12:     if $\widetilde{V}_{ij} < V_{ij}$ then
13:         $V_{ij} \leftarrow \widetilde{V}_{ij}$
14:     end if
15: end for
16: End Initialization
17:
18: while $L$ is nonempty do
19:     Remove the point $\bar{x}$ with the smallest value from $L$.
20:     for $\boldsymbol{x}_{ij} \in N(\bar{x})$ do
21:         Compute a temporary value $\widetilde{V}_{ij}$ using the upwinding discretization.
22:         if $\widetilde{V}_{ij} < V_{ij}$ then
23:             $V_{ij} \leftarrow \widetilde{V}_{ij}$
24:         end if
25:         if $\boldsymbol{x}_{ij}$ is $Far$ then
26:             Label $\boldsymbol{x}_{ij}$ as Considered and add it to $L$.
27:         end if
28:     end for
29: end while
```

As explained in section 1.1, the label-setting Dijkstra's method can be considered as a special case of the generic label-correcting algorithm, provided the current smallest node in L is always selected for removal. Of course, in this case it is more efficient to implement L as a binary heap rather than a queue. The same is also true for the Fast Marching Method, and a detailed description of an efficient implementation of the heap-sort data structure can be found in [38]. The re-sorting of *Considered* nodes upon each update involves up to $O(\log M)$ operations, resulting in the overall computational complexity of $O(M \log M)$.

Unfortunately, the discretization (2.1) is only weakly causal: there exists no $\delta > 0$ such that $U^{NE} > \delta + \max(U^N, U^E)$ whenever $U^{NE} > \max(U^N, U^E)$. Thus, no safe "bucket width" can be defined and Dial-like methods are not applicable to the resulting discretized system. In [46] Tsitsiklis introduced a Dial-like method for a similar discretization but using an 8-neighbor stencil. More recently, another Dial-related method for the Eikonal PDE on a uniform grid was introduced in [27]. A more general formula for the safe bucket-width to be used in Dial-like methods on unstructured acute meshes was derived in [47]. Despite their better computational complexity, Dial-like methods often perform slower than Dijkstra-like methods at least on single processor architectures.

Finally, we note another convenient feature of label-setting methods: if the execution of the algorithm is stopped early (before the list L becomes empty), all gridpoints previously removed from L will already have provably correct values. This property (unfortunately not shared by the methods in sections 2.2-2.3) is very useful in a number of applications: e.g., when computing a quickest path from a single source to a single target or in problems of image segmentation [38].

2.2. Fast Sweeping Methods. Suppose all gridpoints in X are ordered. We will slightly abuse the notation by using a single subscript (e.g., $\boldsymbol{x}_i$) to indicate the particular gridpoint's place in that ordering. The double subscript notation (e.g., $\boldsymbol{x}_{ij}$) will be still reserved to indicate the physical location of a gridpoint in the two-dimensional grid.

Consider discretization (2.1) and suppose that the solution U is known for all the gridpoints. Note that for each $\boldsymbol{x}_i$, the value U_i will only depend on one or two of the neighboring values (depending on which quadrant is used for a two-sided update, similar to (2.3), and on whether a one-sided update is employed, similar to (2.2)). This allows us to define a *dependency digraph* G on the vertices $\boldsymbol{x}_1, \ldots, \boldsymbol{x}_M$ with a link from $\boldsymbol{x}_i$ to $\boldsymbol{x}_j$ indicating that U_j is needed to compute U_i. The causality of the discretization (2.1) guarantees that G will always be acyclic. Thus, if we were to order the gridpoints respecting this causality (i.e., with $i > j \implies$ there is no path in G from $\boldsymbol{x}_j$ to $\boldsymbol{x}_i$), then a single Gauss-Seidel iteration would correctly solve the full system in $O(M)$ operations.

However, unless U was already computed, the dependency digraph G will not be generally known in advance. Thus, basing a gridpoint ordering on it is not a practical option. Instead, one can alternate through a list of several "likely" orderings while performing Gauss-Seidel iterations. A geometric interpretation of the optimal control problem provides a natural list of likely orderings: if all characteristics point from SW to NE, then ordering the gridpoints bottom-to-top and left-to-right within each row will ensure the convergence in a single iteration (a "SW sweep"). The "Fast Sweeping Methods" perform Gauss-Seidel iterations on the system (2.1) in alternating directions (sweeps). Let m be the number of gridpoints in the x-direction and n be the number in the y-direction, and $\boldsymbol{x}_{ij}$ will denote a gridpoint in a uniform Cartesian grid on $\Omega \subset R^2$. For simplicity, we will use the Matlab index notation to describe the ordering of gridpoints in each sweep. There are four alternating sweeping directions: from SW, from SE, from NE, and from NW. For the above described southwest sweep, the gridpoints $\boldsymbol{x}_{ij}$ will be processed in the following order: `i=1:1:m`, `j=1:1:n`. All four orderings are similarly defined in algorithm 3.

The alternating sweeps are then repeated until convergence. The resulting algorithm is summarized in 4.

Remark 2.2. The idea that alternating the order of Gauss-Seidel sweeps might speed up the convergence is a centerpiece of many fast algorithms. For Euclidean distance computations it was first used by Danielsson in [16]. In the context of general HJB PDEs it was introduced by Boue and Dupuis in [12] for a numerical approximation based on controlled Markov chains. More recently, a number of papers by Cheng, Kao, Osher, Qian, Tsai, and Zhao introduced related Fast Sweeping Methods to speed up the iterative solving of finite-difference discretizations [44, 51, 25]. The key challenge for these methods is to find a provable and explicit upper bound on the number of iterations. As of right now, such a bound is only available for boundary value problems in which characteristics are straight lines. Experimental evidence suggests that these methods can be also very efficient for other problems where the characteristics are "largely" straight. The number of necessary iterations is largely independent of M and correlated with the number of times the characteristics

Algorithm 3 Sweeping Order Selection pseudocode.

```
1: $sweepDirection \leftarrow sweepNumber \ \texttt{mod} \ 4$
2: if $sweepDirection == 0$ then
3:     $iOrder \leftarrow \ (1:1:m)$
4:     $jOrder \leftarrow \ (1:1:n)$
5: else if $sweepDirection == 1$ then
6:     $iOrder \leftarrow \ (1:1:m)$
7:     $jOrder \leftarrow \ (n:-1:1)$
8: else if $sweepDirection == 2$ then
9:     $iOrder \leftarrow \ (m:-1:1)$
10:    $jOrder \leftarrow \ (n:-1:1)$
11: else
12:    $iOrder \leftarrow \ (m:-1:1)$
13:    $jOrder \leftarrow \ (1:1:n)$
14: end if
```

Algorithm 4 Fast Sweeping Method pseudocode.

```
1: Initialization:
2: for each gridpoint $\boldsymbol{x}_{ij} \in X$ do
3:     if $\boldsymbol{x}_{ij} \in Q$ then
4:         $V_{ij} \leftarrow q(\boldsymbol{x}_{ij})$.
5:     else
6:         $V_{ij} \leftarrow \infty$.
7:     end if
8: end for
9:
10: Main Loop:
11: sweepNumber ← 0
12: repeat
13:     changed ← FALSE
14:     Determine iOrder and jOrder based on sweepNumber
15:     for $i = iOrder$ do
16:         for $j = jOrder$ do
17:             if $\boldsymbol{x}_{ij} \notin Q$ then
18:                 Compute a temporary value $\widetilde{V}_{ij}$ using upwinding discretization (2.1).
19:                 if $\widetilde{V}_{ij} < V_{ij}$ then
20:                     $V_{ij} \leftarrow \widetilde{V}_{ij}$
21:                     changed ← TRUE
22:                 end if
23:             end if
24:         end for
25:     end for
26:     sweepNumber ← sweepNumber + 1
27: until changed == FALSE
```

"switch directions" (i.e., change from one directional quadrant to another) inside Ω. However, since the quadrants are defined relative to the grid orientation, the number of iterations will generally be grid-dependent.

One frequently encountered argument is that, due to its $O(M)$ computational complexity, the Fast Sweeping is more efficient than the Fast Marching, whose complexity is $O(M \log M)$. However, this asymptotic complexity notation hides constant factors – including this not-easily-quantifiable (and grid-orientation-dependant) bound on the number of iterations needed in Fast Sweeping. As a result, whether the $O(M)$ asymptotic complexity actually leads to any performance advantage on grids of realistic size is a highly problem-dependent question. Extensive experimental comparisons of Marching and Sweeping approaches can be found in [23, 22]. Even though such a comparison is not the main focus of the current paper, the performance of both methods is also tabulated for all examples in section 4. On the grids we tested, we observe that the Fast Marching Method usually performs better than the Fast Sweeping when the domain has a complicated geometry (e.g., shortest/quickest path computations in a maze) or if the characteristic directions change often throughout the domain – the latter situation frequently arises in Eikonal problems when the speed function F is highly inhomogeneous.

We note that the sweeping approach can be in principle useful for a much wider class of problems. For example, the method introduced in [25] is applicable to problems with non-convex Hamiltonians corresponding to differential games; however, the amount of required artificial viscosity is strongly problem-dependent and the choice of consistently discretized boundary conditions can be complicated. Sweeping algorithms for discontinuous Galerkin finite element discretizations of the Eikonal PDE can be found in [30, 50].

The Fast Sweeping Method performs particularly well on problems where the speed function F is constant, since in this case the characteristics of the Eikonal PDE will be straight lines regardless of the boundary conditions. (E.g., if $q \equiv 0$, then the quickest path is a straight line to the nearest boundary point.) As a result, the domain consists of 4 subdomains, each with its own characteristic "quadrant direction". Even though these subdomains are generally not known in advance, it is natural to expect Fast Sweeping to converge in at most 4 iterations (e.g., if $\boldsymbol{x}_{ij}$'s characteristic comes from the SE, then the same is true for all points immediately to SE from $\boldsymbol{x}_{ij}$). However, on the grid, the dependency graph can be more complicated – $\boldsymbol{x}_{ij}$ will depend on both its southern and eastern neighbors. The characteristic directions are changing continuously everywhere, except at the shocks. So, if $\boldsymbol{x}_{ij}$ is near a shock line, one of its neighbors might be in another subdomain, making additional sweeps occasionally necessary even for such simple problems; see Figure 2.1 for an illustration.

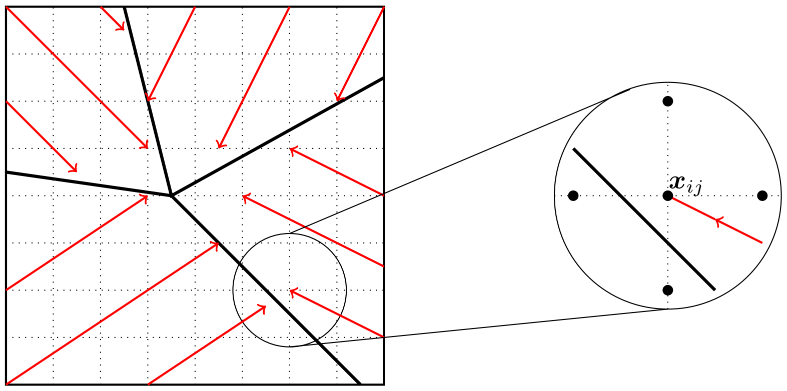

Fig. 2.1. *Four subdomains with a different update quadrant in each of them. If the sweeping directions are used in the order (SE, SW, NW, NE), then the node labeled $\boldsymbol{x}_{ij}$ near the shock line will not receive its final update until the 5th sweep, since its southern neighbor lies in the southwest subdomain. For simplicity, this example uses boundary conditions such that the characteristic directions are constant in each subdomain. As a result, all subdomain boundaries coincide with shock lines, which need not be the case in general, but the illustrated effect is generic.*

Nevertheless, when F is constant, the Fast Sweeping is usually more efficient than the Fast Marching regardless of the boundary conditions – an observation which is the basis for the hybrid methods introduced in the next section.

Remark 2.3. It might seem that the recomputation of V_{ij} from (2.1) will generally require solving 4 quadratic equations to compare the updates from all 4 quadrants. However, the monotonicity property noted in Remark 2.1 guarantees that only one quadrant needs to be considered. E.g., if $U_S < U_N$ then $U^{SE} \leq U^{NE}$ and the latter is irrelevant even if we are currently sweeping from NE. Thus, the relevant quadrant can be always found by using $\min(U_S, U_N)$ and $\min(U_E, U_W)$. We note that this shortcut is not directly applicable to discretizations on unstructured meshes nor for more general PDEs. Interestingly, Alton and Mitchell showed that the same shortcut can also be used with Cartesian grid discretizations of Hamilton-Jacobi PDEs with grid-aligned anisotropy [2].

Remark 2.4. One of the problems in this basic version of the Fast Sweeping Method is the fact that the CPU time might be wasted to recompute V_{ij} even if none of $\boldsymbol{x}_{ij}$'s neighbors have changed since the last sweep. To address this, one natural modification is to introduce "locking flags" for individual gridpoints and to update the currently unlocked gridpoints only [3]. Briefly, all gridpoints but those immediately adjacent to Q start out as locked. When an unlocked gridpoint $\boldsymbol{x}_{ij}$ is processed during a sweep, if U_{ij} changes, then all of its larger neighbors are unlocked. The gridpoint $\boldsymbol{x}_{ij}$ is then itself locked regardless of whether updating U_{ij} resulted in unlocking a neighbor.

The above modification does not change the asymptotic complexity of the method nor the total number of sweeps needed for convergence. Nevertheless, the extra time and memory required to maintain and update the locking flags are typically worthwhile since their use allows to decrease the amount of CPU-time wasted on parts of the domain, where the iterative process already produced the correct numerical solutions. In sections 3 and 4 we will refer to this modified version as Locking Sweeping Method (LSM) to distinguish it from the standard implementation of the FSM.

2.3. Other fast methods for Eikonal equations. Ideas behind many label-correcting algorithms on graphs have also been applied to discretizations of Eikonal PDEs. Here we aim to briefly highlight some of these connections.

Perhaps the first label-correcting methods developed for the Eikonal PDE were introduced by Polymenakos, Bertsekas, and Tsitsiklis based on the logic of the discrete SLF/LLL algorithms [34]. On the other hand, Bellman-Ford is probably the simplest label-correcting approach and it has been recently re-invented by several numerical analysts working with Eikonal and more general Hamilton-Jacobi-Bellman PDEs [11], [3], including implementations for massively parallel computer architectures [24]. A recent paper by Bak, McLaughlin, and Renzi [3] also introduces another "2-queues method" essentially mimicking the logic of thresholding label-correcting algorithms on graphs. While such algorithms clearly have promise and some numerical comparisons of them with sweeping and marching techniques are already presented in the above references, more careful analysis and testing is required to determine the types of examples on which they are the most efficient.

All of the above methods produce the exact same numerical solutions as FMM and FSM. In contrast, two of the three new methods introduced in section 3 aim to gain efficiency even if it results in small additional errors. We know of only one prior numerical method for Eikonal PDEs with a similar trade-off: in [49] a Dial-like method is used with buckets of unjustified width δ for a discretization that is not δ-causal. This introduces additional errors (analyzed in [35]), but decreases the method's running time. However, the fundamental idea behind our new two-scale methods is quite different, since we aim to exploit the geometric structure of the speed function.

3. New hybrid (two-scale) fast methods. We present three new hybrid methods based on splitting the domain into a collection of non-overlapping rectangular "cells" and running the Fast Sweeping Method on individual cells sequentially. The motivation for this decomposition is to break the problem into sub-problems, with F nearly constant inside each cell. If the characteristics rarely change their quadrant-directions within a single cell, then a small number of sweeps should be sufficient on that cell. But to compute the value function correctly within each cell, the correct boundary conditions (coming from the adjacent cells) should be already available. In other words, we need to establish a causality-respecting order for processing the cells. The Fast Marching Sweeping Method (FMSM) uses the cell-ordering found by running the Fast Marching Method on a coarser grid, while the Heap-Cell Methods (HCM and FHCM) determine the cell-ordering dynamically, based on the value-updates on cell-boundaries.

3.1. Fast Marching-Sweeping Method (FMSM). This algorithm uses a coarse grid and a fine grid. Each "coarse gridpoint" is taken to be the center of a cell of "fine gridpoints". (For simplicity, we will assume that the exit-set Q is directly representable by coarse gridpoints.) The Fast Marching is used on the coarse grid, and the Acceptance-order of "coarse gridpoints" is recorded. The Fast Sweeping is then used on the corresponding cells in the same order. An additional speed-up is obtained, by running a fixed number of sweeps on each cell, based on the upwind directions determined on the coarse grid. Before providing the details of our implementation, we introduce some relevant notation:

• $X^c = \{\boldsymbol{x}_1^c, ..., \boldsymbol{x}_J^c\}$, the coarse grid.
• $X^f = \{\boldsymbol{x}_1^f, ..., \boldsymbol{x}_M^f\}$, the fine grid (same as the grid used in FMM or FSM).
• $Q^c \subset X^c$, the set of coarse gridpoints discretizing the exit set Q.
• U^c, the solution of the discretized equations on the coarse grid.
• V^c, the temporary label of the coarse gridpoints.
• $Z = \{c_1, ..., c_J\}$, the set of cells, whose centers correspond to coarse gridpoints.
• $N^c(c_i)$, the neighbors of cell c_i; i.e., the cells that exist to the north, south, east, and west of c_i. (The set $N^c(c_i)$ may contain less than four elements if c_i is a boundary cell.)
• $N^f(c_i)$, the fine grid neighbors of c_i; i.e., $N^f(c_i) = \{\boldsymbol{x}_j^f \in X^f \mid \boldsymbol{x}_j^f \notin c_i \text{ and } N(\boldsymbol{x}_j^f) \bigcap c_i \neq \emptyset\}$.
• $P : \{1, ..., J\} \to \{1, ..., J\}$, a permutation on the coarse gridpoint indices.
• h_x^c, the distance along the x-direction between two neighboring coarse gridpoint.
Assume for simplicity that $h_x^c = h_y^c = h^c$.

All the obvious analogs hold for the fine grid (U^f, h^f, etc). Since Fast Marching will be used on the coarse grid only, the heap L will contain coarse gridpoints only.

Algorithm 5 Fast Marching-Sweeping Method pseudocode.

```
Part I:
Run FMM on $X^c$ (see algorithm 2).
Build the ordering $P$ to reflect the Acceptance-order on $X^c$.

Part II:
Fine grid initialization:
for each gridpoint $\boldsymbol{x}_i^f \in X^f$ do
    if $\boldsymbol{x}_i^f \in Q^f$ then
        $V_i^f \leftarrow q_i^f$;
    else
        $V_i^f \leftarrow \infty$;
    end if
end for

for $j = P(1) : P(J)$ do
    Define the fine-grid domain $\tilde{c} = c_j \bigcup N^f(c_j)$.
    Define the boundary condition as
            $\tilde{q}(\boldsymbol{x}_i^f) = q(\boldsymbol{x}_i^f)$ on $c_j \bigcap Q^f$ and
            $\tilde{q}(\boldsymbol{x}_i^f) = V_i^f$ on $N^f(c_j)$.
    Perform Modified Fast Sweeping (see Remark 3.1) on $\tilde{c}$ using boundary conditions $\tilde{q}$.
end for
```

Remark 3.1. The "Modified Fast Sweeping" procedure applied to individual cells in the algorithm 5 follows the same idea as the FSM described in section 2.2. For all the cells containing parts of Q (i.e., the ones whose centers are Accepted *in the initialization* of the FMM on the coarse grid) we use the FSM without any changes. For all the remaining cells, our implementation has 3 important distinctions from the algorithm 4:

1. No initialization of the fine gridpoints within $\tilde{c}$ is needed since the entire fine grid is pre-initialized in advance.
2. Instead of looping through different sweeps until convergence, we use at most four sweeps and only in the directions found to be "upwind" on the coarse grid. As illustrated by Figure 3.1, the cells in $N^c(c_i)$ whose centers were accepted prior to $\boldsymbol{x}_i^c$ determine the sweep directions to be used on c_i.
3. When computing V_i^f during the sweeping, we do not employ the procedure described in Remark 2.3 to find the relevant quadrant. Instead, we use "sweep-directional updates"; e.g.,

if the current sweeping direction is from the NE, we always use the update based on the northern and eastern neighboring fine gridpoints. The advantage is that we have already processed both of them within the same sweep.

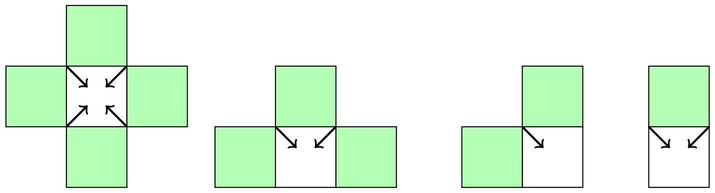

FIG. 3.1. *Sweeping directions on c_i chosen based on the neighboring cells accepted earlier than c_i (shown in green). Note that 2 sweeping directions are conservatively used in the case of a single accepted neighbor.*

Before discussing the computational cost and accuracy consequences of these implementation choices, we illustrate the algorithm on a specific example: a checkerboard domain with the speed function $F = 1$ in white and $F = 2$ in black checkers, and the exit set is a single point in the center of the domain see Figure 3.2). This example was considered in detail in [32]; the numerical results and the performance of our new methods on the related test problems are described in detail in section 4.2. As explained in Remark 3.1.2, we do not sweep until convergence on each cell; e.g., the sweeps for the cell # 1 in Figure 3.2 will be from northwest and southwest, while the cell #14 will be swept from northeast only.

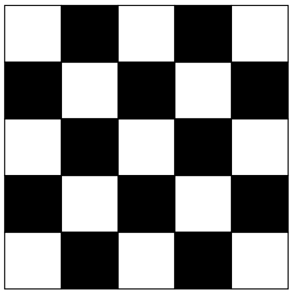

21	18	12	19	24
15	7	3	6	16
10	2	0	1	11
14	8	4	5	13
23	17	9	20	22

FIG. 3.2. *Left: The 5×5 checkerboard domain with a source point in the slow checker in the center. Right: The order of cell-acceptance in Part I of FMSM, assuming that the size of cells and checker is the same.*

The resulting algorithm clearly introduces additional numerical errors – in all but the simplest examples, the FMSM's output is not the exact solution of the discretized system (2.1) on X^f. We identify three sources of additional errors: the fact that the coarse grid computation does not capture all cell interdependencies, and the two cell-sweeping modifications described in Remark 3.1. Of these, the first one is by far the most important. Focusing on the fine grid, we will say that the cell c_i *depends on* $c_j \in N^c(c_i)$ if there exists a gridpoint $\boldsymbol{x}_k^f \in c_i$ such that U_k^f directly depends on U_l^f for some gridpoint $\boldsymbol{x}_l^f \in c_j$. In the limit, as $h^f \to 0$, this means that c_i depends on c_j if there is a characteristic going from c_j into c_i (i.e., at least a part of c_i's boundary shared with c_j is *inflow*). For a specific speed function F and a fixed cell-decomposition Z, a causal ordering of the cells need not exist at all. As shown in Figure 3.3, two cells may easily depend on each other. This situation arises even for problems where F is constant on each cell; see Figure 4.2. Moreover, if the cell refinement is performed uniformly, such non-causal interdependencies will be present even as the cell size $h^c \to 0$. This means that every algorithm processing each cell only once (or even a fixed number of times) will unavoidably introduce additional errors at least for some speed functions F.

One possible way around this problem is to use the characteristic's vacillations between c_i to c_j to determine the total number of times that these cells should be alternately processed with FSM. This idea is the basis for heap-cell methods described in the next section. However, for the FMSM we simply treat these "approximate cell-causality" errors as a price to pay for the higher computational efficiency. Our numerical experiments with FMSM showed that, as $h^c \to 0$, the effects due to the approximate cell-causality dominate the errors stemming from using a finite (coarse-grid determined)

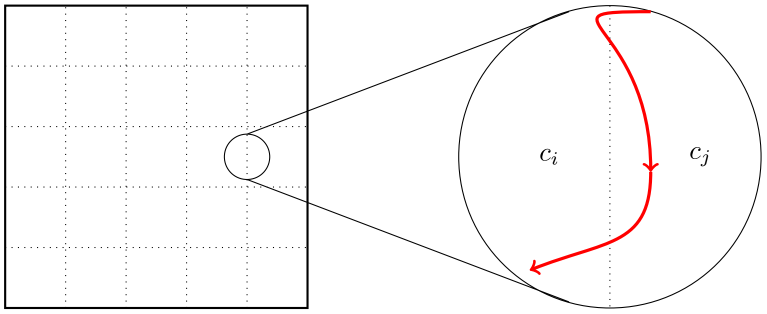

FIG. 3.3. *Two mutually dependent cells.*

number of sweeps. I.e., when the cells are sufficiently small, running FSM to convergence does not decrease the additional errors significantly, but does noticeably increase the computational cost. The computational savings due to our use of "sweep-directional updates" are more modest (we simply avoid the necessity to examine/compare all neighbors of the updated node), but the numerical evidence indicates that it introduces only small additional errors and only near the shock lines, where ∇u is undefined. Since characteristics do not emanate from shocks, the accuracy price of this modification is even more limited if the errors are measured in L_1 norm. In section 4 we show that on most of X^f the cumulative additional errors in FMSM are typically much smaller than the discretization errors, provided h^c is sufficiently small.

The monotonicity property of the discretization ensures that the computed solution V^f will always satisfy $V_i^f \geq U_i$. The numerical evidence suggests that V^f becomes closer to U^f as h^c decreases, though this process is not always monotone.

The computational cost of Part I is relatively small as long as $J \ll M$. However, if h^f and M are held constant while h^c decreases, this results in $J \to M$, and the total computational cost of FMSM eventually increases. As of right now, we do not have any method for predicting the optimal h^c for each specific example. Such a criterion would be obviously useful for realistic applications of our hybrid methods, and we hope to address it in the future.

3.2. Label-correcting methods on cells. The methods presented in this section also rely on the cell-decomposition $Z = \{c_1, \ldots, c_J\}$, but do not use any coarse-level grid. Thus, $X = X^f$ and we will omit the superscripts f and c with the exception of $N^c(c_i)$ and $N^f(c_i)$. We will also use h^c to denote the distance between the centers of two adjacent square cells. In what follows, we will also define "cell values" to represent coarse-level information about cell dependencies. Unlike in finite volume literature, here a "cell value" is not necessarily synonymous with the average of a function over a cell.

3.2.1. A generic cell-level convergent method. To highlight the fundamental idea, we start with a simple "generic" version of a label-correcting method on cells. We maintain a list of cells to be updated, starting with the cells containing the exit set Q. While the list is non-empty, we choose a cell to remove from it, "process" that cell (by any convergent Eikonal-solver), and use the new grid values near the cell boundary to determine which neighboring cells should be added to the list. The criterion for adding cells to the list is illustrated in Figure 3.4. All other implementation details are summarized in Algorithm 6.

It is easy to prove by induction that this method terminates in a finite number of steps; in Theorem 3.2 we show that upon its termination $V = U$ on the entire grid X, regardless of the specific Eikonal-solver employed to process individual cells (e.g., FMM, FSM, LSM or any other method producing the exact solution to (2.1) will do). We emphasize that the fact of convergence also does not depend on the specific selection criteria for the next cell to be removed from L. However, even for a fixed cell-decomposition Z, the above choices will significantly influence the total number of list removals and the overall computational cost of the algorithm. One simple strategy is to implement L as a queue, adding cells at the bottom and always removing from the top, thus mirroring the logic of Bellman-Ford algorithm. In practice, we found the version described in the next subsection to be

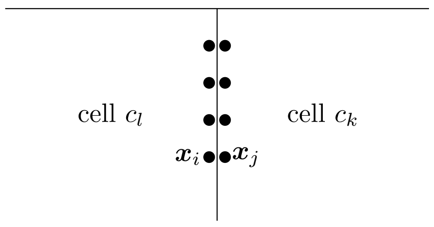

FIG. 3.4. *Suppose that, as a result of processing the cell c_l an eastern border value V_i becomes updated. If $V_i < V_j$ and $\boldsymbol{x}_j \notin Q$, the cell c_k will be added to L (unless it is already on the list).*

Algorithm 6 Generic Label-Correcting on Cells pseudocode.

```
1:  Cell Initialization:
2:  for each cell $c_k$ do
3:      if $c_k \cap Q \neq \emptyset$ then
4:          add $c_k$ to the list $L$
5:      end if
6:  end for
7:
8:  Fine Grid Initialization:
9:  for each gridpoint $\boldsymbol{x}_i$ do
10:     if $\boldsymbol{x}_i \in Q$ then
11:         $V_i \leftarrow q(\boldsymbol{x}_i)$
12:     else
13:         $V_i \leftarrow \infty$
14:     end if
15: end for
16:
17: Main Loop:
18: while $L$ is nonempty do
19:     Remove a cell $c$ from the list $L$.
20:     Define a domain $\tilde{c} = c \cup N^f(c)$.
21:     Define the boundary condition as
22:             $\tilde{q}(\boldsymbol{x}_i) = q(\boldsymbol{x}_i)$ on $c \cap Q$ and
23:             $\tilde{q}(\boldsymbol{x}_i) = V_i$ on $N^f(c)$.
24:     Process $c$ by solving the Eikonal on $\tilde{c}$ using boundary conditions $\tilde{q}$.
25:     for each cell $c_k \in N^c(c) \backslash L$ do
26:         if $\exists\, \boldsymbol{x}_i \in \left(c \cap N^f(c_k)\right)$ AND $\boldsymbol{x}_j \in (c_k \cap N(\boldsymbol{x}_i) \backslash Q)$ such that
                ( $V_i$ has changed OR ($\boldsymbol{x}_i \in Q$ AND $c$ is removed from $L$ for the first time) )
                AND ($V_i < V_j$) then
27:             Add $c_k$ to the list $L$.
28:         end if
29:     end for
30: end while
```

more efficient.

THEOREM 3.2. *The generic cell-based label-correcting method converges to the exact solution of system* (2.1).

Proof.

First we describe notation and recall from section 2.2 the dependency digraph G.

• We say $\boldsymbol{x}_j$ *depends on* $\boldsymbol{x}_i$ if U_i is used to compute U_j (see discussion of formulas (2.2) and (2.3)).

• $\Gamma_{\boldsymbol{x}} = \{$nodes in G on which $\boldsymbol{x}$ depends directly$\}$. For each node $\boldsymbol{x}$, the set $\Gamma_{\boldsymbol{x}}$ will have 0, 1, or 2 elements. If $\boldsymbol{x} \in Q$, then $\Gamma_{\boldsymbol{x}}$ is empty. If a one-sided update was used to compute $U(\boldsymbol{x})$ (see

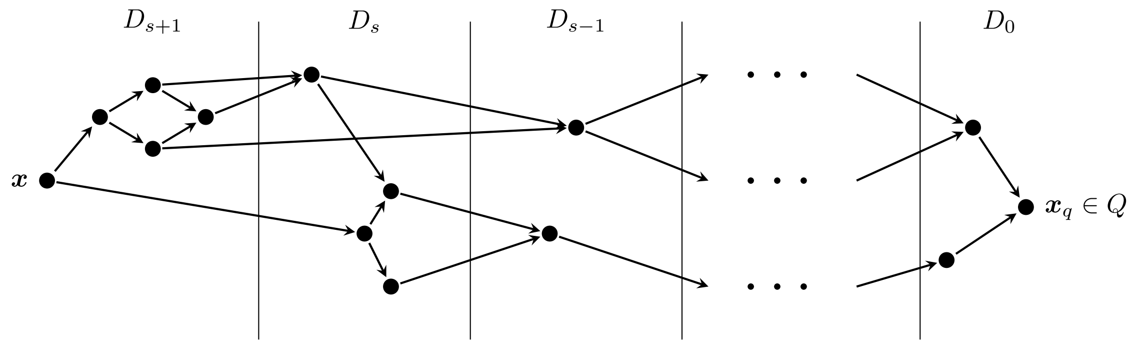

FIG. 3.5. *A schematic view of dependency digraph $G_{\boldsymbol{x}}$.*

formula (2.2)), then there is only one element in $\Gamma_{\boldsymbol{x}}$.

- $G_{\boldsymbol{x}}$ denotes the subgraph of G that is reachable from the node $\boldsymbol{x}$.
- We define the cell transition distance $d(\boldsymbol{x}) = max_{\boldsymbol{x}_i \in \Gamma_{\boldsymbol{x}}}\{d(\boldsymbol{x}_i)+$ cell_dist$(\boldsymbol{x}, \boldsymbol{x}_i)\}$,

where cell_dist$(\boldsymbol{x}, \boldsymbol{x}_i) = 0$ if both $\boldsymbol{x}$ and $\boldsymbol{x}_i$ are in the same cell and 1 otherwise. Note that in general $d(\boldsymbol{x}) < M$, but in practice $\max d(\boldsymbol{x})$ is typically much smaller. In the continuous limit $d(\boldsymbol{x})$ is related to the number of times a characteristic that reaches $\boldsymbol{x}$ crosses cell boundaries.

- $D_s = \{\boldsymbol{x} \in G \mid d(\boldsymbol{x}) = s\}$. See Figure 3.5 for an illustration of $G_{\boldsymbol{x}}$ split into $D_0, D_1, \ldots, D_{d(\boldsymbol{x})}$.
- $\widetilde{D}_s = \{\boldsymbol{x}_j \in D_s \mid \exists \boldsymbol{x}_i \in D_{s-1}$ such that $\boldsymbol{x}_j$ depends on $\boldsymbol{x}_i\}$, i.e., the set of gridpoints in D_s that depend on a gridpoint in a neighboring cell. Note that $\widetilde{D}_0 = \emptyset$.
- $\widehat{D}_s = \{\boldsymbol{x}_i \in D_s \mid \exists \boldsymbol{x}_j \in D_{s+1}$ such that $\boldsymbol{x}_j$ depends on $\boldsymbol{x}_i\}$, i.e., the set of gridpoints in D_s that influence a gridpoint in a neighboring cell.
- $\star$ denotes any method that exactly solves the Eikonal on $\tilde{c}$ (see line 20 of algorithm 6).

Recall that by the monotonicity property of the discretization (2.1), the temporary labels V_j will always be greater than or equal to U_j throughout algorithm 6. Moreover, once V_j becomes equal to U_j, this temporary label will not change in any subsequent applications of $\star$ to the cell c containing $\boldsymbol{x}_j$. The goal is to show that $V_j = U_j$ for all $\boldsymbol{x}_j \in X$ upon the termination of Algorithm 6.

To prove convergence we will use induction on s. First, consider $s = 0$ and note that every cell c containing some part of D_0 is put in L at the time of the cell initialization step of the algorithm. When c is removed from L and $\star$ is applied to it, every $\boldsymbol{x} \in D_0 \cap c$ will obtain its final value $V(\boldsymbol{x}) = U(\boldsymbol{x})$ because $G_{\boldsymbol{x}}$ contains no gridpoints in other cells by the definition of D_0.

Now suppose all $\boldsymbol{x} \in D_k$ already have $V(\boldsymbol{x}) = U(\boldsymbol{x})$ for all $k \leq s$. We claim that:
1) If a cell c contains any $\boldsymbol{x} \in D_{s+1}$ such that $V(\boldsymbol{x}) > U(\boldsymbol{x})$, then this cell is guaranteed to be in L at the point in the algorithm when the last $\boldsymbol{x}_i \in D_s \cap N^f(c)$ receives its final update.
2) The next time $\star$ is applied to c, $V(\boldsymbol{x})$ will become equal to $U(\boldsymbol{x})$ for all $\boldsymbol{x} \in D_{s+1} \cap c$.

To prove 1), suppose $D_{s+1} \cap c \neq \emptyset$ and note that there exist $\boldsymbol{x}_j \in \widetilde{D}_{s+1} \cap c$ and $\boldsymbol{x}_i \in \Gamma_{\boldsymbol{x}_j}$ with $\boldsymbol{x}_i \in \widehat{D_s} \cap \hat{c}$ for some neighboring cell $\hat{c}$. Indeed, if each gridpoint $\boldsymbol{x} \in D_{s+1} \cap c$ were to depend only on those in D_{s+1} (gridpoints within the same cell) and/or those in D_k for $k < s$, this would contradict $\boldsymbol{x} \in D_{s+1}$ (it is not possible for $\Gamma_{\boldsymbol{x}} \subset \cup_{k<s} D_k$; see Figure 3.5). At the time the *last such* $\boldsymbol{x}_i$ receives its final update, we will have $V_j \geq U_j > U_i = V_i$ since $\boldsymbol{x}_i \in \Gamma_{\boldsymbol{x}_j}$. Thus, c is added to L (if not already there) as a result of the add criterion in Algorithm 6.

To prove 2), we simply note that all nodes in $(G_{\boldsymbol{x}} \backslash c) \subset (\bigcup_{k=0}^{s} D_k)$ will already have correct values at this point.
□

REMARK 3.3. We note that the same ideas are certainly applicable to finding shortest paths on graphs. The Algorithm 1 can be similarly modified using a collection of non-overlapping subgraphs instead of cells, but so far we were unable to find any description of this approach in the literature.

3.2.2. Heap-Cell Method (HCM).

To ensure the efficiency of cell-level label-correcting algorithms, it is important to have the "influential" cells (on which most others depend) processed as early as possible. Once the algorithm produces correct solution $V = U$ on those cells, they will never enter the list again, and their neighboring cells will have correct boundary conditions at least on a part of their boundary. The same logic can be applied repeatedly by always selecting for removal the most "influential" cells currently on the list. We introduce the concept of "cell values" $V_k^c = V^c(c_k)$ to estimate the likelihood of that cell influencing others (the smaller is V_k^c, the more likely is c_k to influence subsequent computations in other cells, and the higher is its priority of removal from the list). In Fast Marching-Sweeping Method of section 3.1, the cell values were essentially defined by running FMM on the coarse grid. That approach is not very suitable here, since each cell c_k might enter the list more than once and it is important to re-evaluate V_k^c each time this happens. Instead, we define and update V_k^c using the boundary values in the adjacent cells, and modify Algorithm 6 to use the cell values as follows:

1. Amend the cell initialization to set
$$V_k^c \leftarrow \max_{\boldsymbol{x}_i \in (c_k \cap Q)} q(\boldsymbol{x}_i) \quad \text{or} \quad V_k^c \leftarrow \infty \text{ if } c_k \cap Q = \emptyset.$$
2. Always remove and process the cell with the smallest value currently on the list. Efficient implementation requires maintaining L as a heap-sort data structure – hence the name of "Heap-Cell Method" (HCM) for the resulting algorithm.
3. After solving the Eikonal on c, update the cell values for all $c_k \in N^c(c)$ (including those already in L). Let $\boldsymbol{b}_k$ be a unit vector pointing from the center of c in the direction of c_k's center and suppose that $\boldsymbol{x}_i$ has the largest current value among the gridpoints inside c but adjacent to c_k; i.e., $\boldsymbol{x}_i = \operatorname*{argmax}_{\boldsymbol{x}_j \in (c \cap N^f(c_k))} V_j$. Define $\boldsymbol{y}_i = \boldsymbol{x}_i + \frac{h+h^c}{2}\boldsymbol{b}_k$. Then
$$\begin{aligned} \widetilde{V}_k^c &\leftarrow V_i + \frac{(h+h^c)/2}{F(\boldsymbol{y}_i)}; \\ V_k^c &\leftarrow \min\left(V_k^c, \widetilde{V}_k^c\right). \end{aligned} \tag{3.1}$$

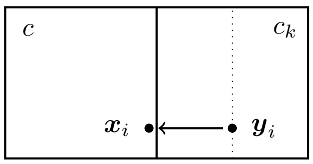

FIG. 3.6. *An illustration corresponding to equation 3.1 (the estimate for a cell value) with* $\boldsymbol{b}_k = (1, 0)$.

REMARK 3.4. We note that, in the original Dijkstra's and Bellman-Ford methods on graphs, a neighboring node's temporary label is updated *before* that node is added to L. In the Heap-Cell Method, the cell value is also updated before adding that cell to the list, but the grid values within that cell are updated *after* it is removed from L.

Regardless of the method used to compute cell values, they can only provide an estimate of the dependency structure. As explained in section 3.1, a causal cell-ordering need not exist for a fixed Z and a general speed functions F. Thus, $V_k^c < V_i^c$ does not exclude the possibility of c_k depending on c_i, and we do not use cell values to decide which neighboring cells to add to the list – this is still done based on the cell boundary data; see Algorithm 6. As a result, the fact of convergence of such cell-level methods does not depend on the particular heuristic used to define cell values. There are certainly many reasonable alternatives to formula (3.1) (e.g., a more aggressive/optimistic version can instead select $\boldsymbol{x}_i = \operatorname{argmin} V_j$ on the boundary; an average value of F on c_k could also be used here; or the distance to travel could be measured from $\boldsymbol{x}_i$ to the center of c_k, etc). Empirically, formula (3.1) results in smaller computational cost than the mentioned alternatives and it was therefore used in our implementation.

REMARK 3.5. The cell-values are useful even if L is implemented as a queue and the cells are always removed from the top. Indeed, V_k^c can still be used to decide whether c_k should be added at the top or at the bottom of L. This is the SLF/LLL strategy previously used to solve the Eikonal PDE on the grid-level (i.e., without any cells) by Polymenakos, Bertsekas, and Tsitsiklis [34]. We have also implemented this strategy and found it to be fairly good, but on average less efficient than the HCM described above. (The performance comparison is omitted to save space.) The intuitive reason is that the SLF/LLL is based on mimicking the logic of Dijkstra's method, but without the expensive heap-sort data structures. However, when $J \ll M$, the cost of maintaining the heap is much smaller than the cost of occasionally removing/processing less influential cells from L.

To complete our description of HCM, we need to specify how the Eikonal PDE is solved on individual cells. Since the key idea behind our hybrid methods is to take advantage of the good performance of sweeping methods when the speed is more or less constant, we follow the same idea as the FSM described in section 2.2, but with the following important distinctions from the basic version of algorithm 4:

1. No initialization of gridpoint values V_i is needed within $\tilde{c}$ – indeed, the initialization is carried out on the full grid at the very beginning and if c is removed from L more than once, the availability of previously computed V_i's might only speed up the convergence on c. Here we take advantage of the comparison principle for the Eikonal PDE: the viscosity solution cannot increase anywhere inside the cell in response to decreasing the cell-boundary values.
2. We use the Locking Sweeping version described in Remark 2.4.
3. The standard FSM and LSM loop through the four sweep directions always in the same order. In our implementation of HCM, we choose a different order for the first four sweeps to ensure that the "preferred sweep directions" (determined for each cell individually) are used before all others. For all other sweeps after the first four, we revert to the standard loop defined in Algorithm 3. Of course, as in the standard FSM, the sweeps only continue as long as grid values keep changing somewhere inside the cell. The procedure for determining preferred sweep directions is explained in Remark 3.6.

Remark 3.6. Recall that in FMSM, the coarse grid information was used to determine the sweep directions to use on each cell; see Remark 3.1 and Figure 3.1. Similarly, in HCM we use the neighboring cells of c_k that were found to have newly changed c_k-inflow boundary since the last time c_k was added to L. We maintain four "directional flags" – boolean variables initialized to `FALSE` and representing all possible preferred sweeping directions – for each cell c_k currently in L. When a neighboring cell c_l is processed/updated and is found to influence c_k, this causes two of c_k's directional flags to be set to `TRUE`. To illustrate, supposing that c_l is a currently-processed-western-neighbor of c_k (as in Figure 3.4). If the value of $\boldsymbol{x}_i \in c_l \cap N^f(c_k)$ has just changed and $V_i < V_j$, then both relevant preferred direction flags in c_k (i.e., both NW and SW) will be raised. Once c_k is removed from L and processed, its directional flags are reset to `FALSE`.

As explained in section 3.2.3, a better procedure for setting these directional flags could be built based on fine-grid information on the cell-boundary. However, we emphasize that the procedure for determining preferred directions will not influence the ultimate output of HCM (since we will sweep on c_k until convergence every time we remove it from L), though such preferred directions are usually useful in reducing the number of sweeps needed for convergence.

The performance and accuracy data in section 4 shows that, for sufficiently small h and h^c, HCM often outperforms both FMM and FSM on a variety of examples, including those with piecewise continuous speed function F. This is largely due to the fact that the average number of times a cell enters the heap tends to 1 as $h^c \to 0$.

3.2.3. Fast Heap-Cell Method (FHCM).

We also implement an accelerated version of HCM by using the following modifications:

1. Each newly removed cell is processed using at most four iterations – i.e., it is only swept once in each of the preferred directions instead of continuing to iterate until convergence.
2. Directional flags in all cells containing parts of Q are initialized to `TRUE`.
3. To further speed up the process, we use a "Monotonicity Check" on cell-boundary data to further restrict the preferred sweeping directions. For concreteness, assume that c_l and c_k are related as in Figure 3.4. If the grid values in $N^f(c_k) \cap c_l$ are monotone non-decreasing from north to south, we set c_k's NW preferred direction flag to `TRUE`; if those grid values are monotone non-increasing we flag SW; otherwise we flag both NW and SW. (In contrast, both HCM and FMSM are always using two sweeps in this situation; see Figure 3.1 and

Remark 3.6.) We note that the set $c \cap N^f(c_k)$ already had to be examined to compute an update to V_k^c and the above Monotonicity Check can be performed simultaneously.

The resulting Fast Heap-Cell Method (FHCM) is significantly faster than HCM, but at the cost of introducing additional errors (see section 4).

The Monotonicity Checks result in a considerable increase in performance since, for small enough h^c, most cell boundaries become monotone. However, generalizing this procedure to higher dimensional cells is less straightforward. For this reason we decided against using Monotonicity Checks in our implementation of HCM. FHCM is summarized in Algorithm 7.

Algorithm 7 Fast Heap-Cell Method pseudocode.

```
1: Cell Initialization:
2: **if** cell $c_k \ni \boldsymbol{x}$ for $\boldsymbol{x} \in Q^f$ **then**
3:     Add $c_k$ to the list $L$;
4:     Tag all four sweeping directions of $c_k$ as *true*;
5:     Assign a cell value $V_k^{cell} := 0$;
6: **else**
7:     Assign a cell value $V_k^{cell} := \infty$;
8: **end if**
9: Fine Grid Initialization:
10: **if** $\boldsymbol{x}_i^f \in Q^f$ **then**
11:     $V_i^f := q_i^f$;
12: **else**
13:     $V_i^f := \infty$;
14: **end if**
15:
16: **while** $L$ is nonempty **do**
17:     Remove cell at the top of $L$;
18:     Perform Non-Directional Fast Sweeping within the cell according to its directions marked
        *true*, then set all directions to *false* and:
19:     **for** Each cell border N,S,E,W **do**
20:         **if** the value of a gridpoint $\boldsymbol{x}_i^f$ along a border changes and $V_i^f < V_j^f$ for $\boldsymbol{x}_j^f$ a neighboring
            gridpoint across the border **then**
21:             Add the cell $c_k$ containing $x_j^f$ onto $L$ if not already there.
22:             Update the planned sweeping directions for $c_k$ based on the location of the cell
                containing $\boldsymbol{x}_i^f$ (more about this later).
23:         **end if**
24:         Compute a value $v$ for the neighbor cell $c_k$ (more about this later)
25:         **if** $v < V_k^{cell}$ **then**
26:             $(V_k^{cell}) \leftarrow v$
27:         **end if**
28:     **end for**
29: **end while**
```

As an illustration, we consider another 5×5 checkerboard example (this time with a fast checker in the center) and show the contents of the heap in Figure 3.7.

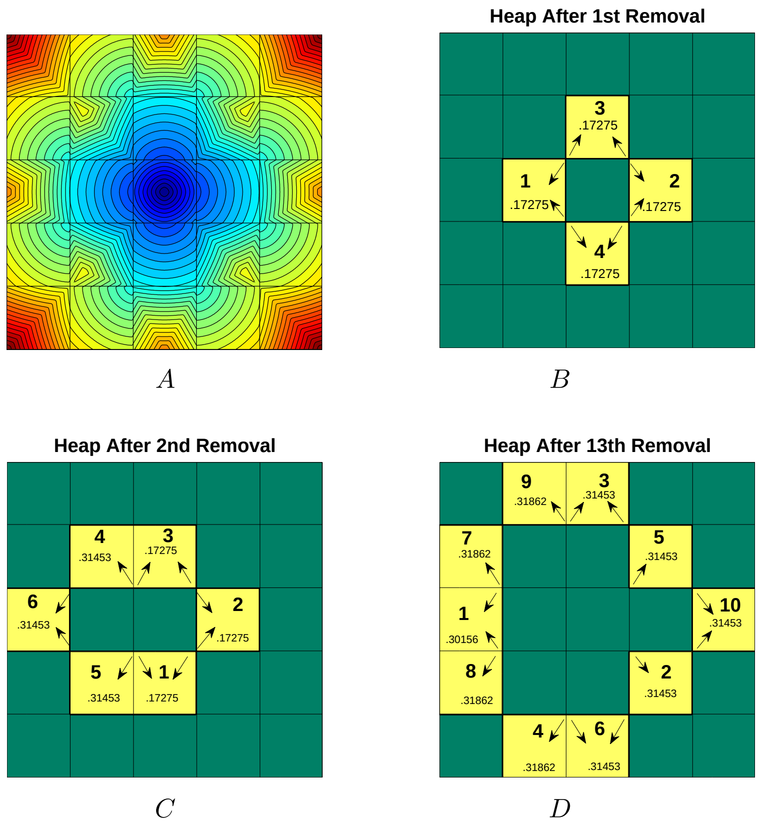

Fig. 3.7. *FHCM on a* 5×5 *checkerboard example. The level sets of the solution are shown in subfigure A. The state of the cell-heap, current cell values and tagged preferred sweeping directions are shown after 1, 2, and 13 cell removals in subfigures B, C, and D.*

Here we take the cells coinciding with checkers; finer cell-decompositions are numerically tested in section 4.2. The arrows indicate flagged sweeping directions for each cell, and the smaller font is used to show the current cell values. Similarly to Dijkstra's method and FMM, the heap data structure is implemented as an array; the bold numbers represent each cell's index in this array. In the beginning the central cell is the only one in L; once it is removed, it adds to L all four of its neighbors, all of them with the same cell value. Once the first of these (to the west of the center) is removed, it adds three more neighbors[3] (but not the central cell since there are no characteristics passing through the former into the latter). This is similar to the execution path of FMSM, however, with heap-cell methods the cells may generally enter the heap more than once. Thus, additional errors introduced by FHCM are usually smaller than those in FMSM.

Remark 3.7. To conclude the discussion of our heap-cell methods, we briefly describe a recent algorithm with many similar features, but very different goals and implementation details. The "Raster scan algorithm on a multi-chart geometry image" was introduced in [48] for geodesic distance computations on parametric surfaces. Such surfaces are frequently represented by an atlas of overlapping charts, where each chart has its own parametric representation and grid resolution (depending on the detail level of the underlying surface). The computational subdomains corresponding to charts are typically large and the "raster scan algorithm" (similar to the traditional FSM with a fixed ordering of sweep directions) is used to parallelize the computations within each chart. The heuristically defined chart values are employed to decide which chart will be raster-scanned next.

[3]We note that the cell indexed 4 after the first removal is indexed 2 immediately after the second. This is the consequence of the performing *remove_the_smallest* using the *down_heap* procedure in the standard implementation of the heap; see [39].

Aside from the difference in heuristic formulas used to compute chart values, in [48] the emphasis is on providing the most efficient implementation of raster scans on each chart (particularly for massively parallel architectures). The use of several large, parametrization/resolution-defined charts, typically results in complicated chart interdependencies since most chart boundaries are generally both inflow and outflow. Moreover, if this method is applied to any Eikonal problems beyond the geodesic distance computations, the monotonicity of characteristic directions will generally not hold and a high number of sweeps may be needed on each chart. In contrast, our focus is on reducing the cell interdependencies and on the most efficient cell ordering: when h^c is sufficiently small, most cell boundaries are either completely inflow or outflow, defining a causal relationship among the cells. Relatively small cell sizes also ensure that F is approximately constant, the characteristics are approximately straight lines, and only a small number of sweeps is needed on each cell. Finally, the cell orderings are also useful to accelerate the convergence within each cell by altering the sweep-ordering based on the location of upwinding cells (as in FMSM and HCM) or based on fine-grid cell-boundary data (as in FHCM). The hybrid methods introduced here show that causality-respecting domain decompositions can accelerate even serial algorithms on single processor machines.

4. Numerical Experiments. All examples were computed on a unit square $[0,1]\times[0,1]$ domain with zero boundary conditions $q=0$ on the exit set Q (defined separately in each case). In each example that follows we have fixed the grid size $h=h^f$, and only the cell size h^c is varied. Since analytic formulas for viscosity solutions are typically unavailable, we have used the Fast Marching Method on a much finer grid (of size $h/4$) to obtain the "ground truth" used to evaluate the errors in all the other methods.

Suppose e_i is the absolute value of the error-due-to-discretization at gridpoint $\boldsymbol{x}_i$ (i.e., the error produced by FSM or FMM when directly executed on the fine grid), and suppose E_i is the absolute value of the error committed by one of the new hybrid methods at the same $\boldsymbol{x}_i$. Define the set $X_+=\{\boldsymbol{x}_i\in X \mid e_i\neq 0\}$ and let $M_+=|X_+|$ be the number of elements in it. (We verified that $\boldsymbol{x}_i\notin X_+ \Rightarrow E_i=0$ in all computational experiments.) To analyze the "additional errors" introduced by FMSM and FHCM, we report
• the *Maximum Error Ratio* defined as $\mathcal{R}=\max_i(E_i/e_i)$, where the maximum is taken over $\boldsymbol{x}_i\in X_+$;
• the *Average Error Ratio* defined as $\rho=\frac{\sum(E_i/e_i)}{M_+}$, where the sum is taken over $\boldsymbol{x}_i\in X_+$;
• the *Ratio of Maximum Errors* defined as $R=\frac{\max_i(E_i)}{\max_i(e_i)}$.
R is relevant since on parts of the domain where e_i's are very small, additional errors might result in large $\mathcal{R}$ even if E_i's are quite small compared to the L_∞ norm of discretization errors. In the ideal scenario, with no additional errors, $\mathcal{R}=\rho=R=1$.
For the Heap-Cell algorithms we also report
• *AvHR*, the average number of heap removals per cell,
• *AvS*, the average number of sweeps per cell, and
• *Mon %*, the percentage of times that the "cell-boundary monotonicity" check was successful.
Finally, we report the number of sweeps needed in FSM and LSM for each problem.

Remark 4.1. Performance analysis of competing numerical methods is an obviously delicate undertaking since the implementation details as well as the choice of test problems might affect the outcome. We have made every effort to select representative examples highlighting advantages and disadvantages of all approaches. All tests were performed on an AMD Turion 2GHz dual-core processor with 3GB RAM. Only one core was used to perform all tests. Our C++ implementations were carefully checked for the efficiency of data structures and algorithms, but we did not conduct any additional performance tuning or Assembly-level optimizations. Our code was compiled using the `g++` compiler version 3.4.2 with compiler options `-O0 -finline`. We have also preformed all tests with the full compiler optimization (i.e., with `-O3`); the results were qualitatively similar, but we opted to report the performance data for the unoptimized version to make the comparison as compiler-independent as possible. For each method, all memory allocations (for grids and heap data structures) were not timed; the reported CPU times include the time needed to initialize the relevant data structures and run the corresponding algorithm. We also note that the speed function $F(\boldsymbol{x})$ was computed by a separate function call whenever needed, rather than precomputed and stored for every gridpoint during initialization. All CPU-times are reported in seconds for the Fast Marching

(FMM), the standard Fast Sweeping (FSM), the Locking Sweeping (LSM), and the three new hybrid methods (HCM, FHCM, and FMSM).

4.1. Comb Mazes. The following examples model optimal motion through a maze with slowly permeable barriers. Speed function $F(x, y)$ is defined by a "comb maze": $F = 1$ outside and 0.01 inside the barriers; see Figure 4.1. The exit set consists of the origin: $Q = \{(0, 0)\}$. The computational cost of sweeping methods is roughly proportional to the number of barriers, while FMM is only minimally influenced by this. The same good property is inherited by the hybrid methods introduced in this paper. The first example with 4 barriers uses barrier walls aligned with cell boundaries and all hybrid methods easily outperform the fastest of the previous methods (LSM); see Table 4.1.

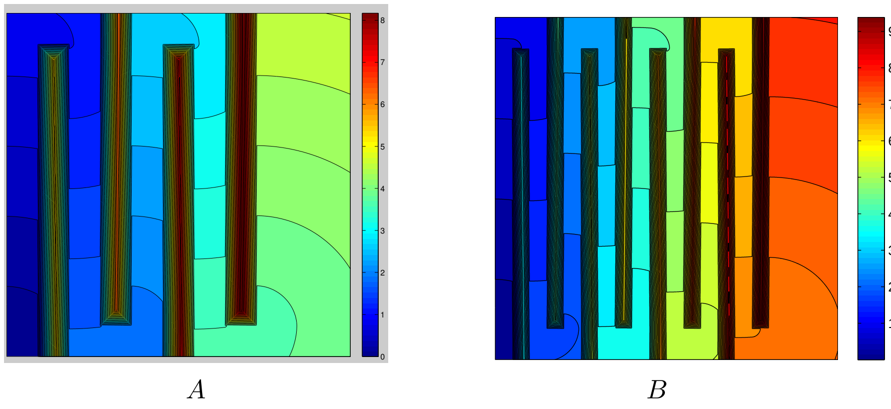

Fig. 4.1. *Min time to the point* $(0, 0)$ *on comb maze domains: 4 barriers (A), and 8 barriers (B).*

Table 4.1
Performance/convergence results for a 4 wall comb maze example.

Grid Size	**L_∞ Error**	**L_1 Error**	**FMM Time**	**FSM Time**	**LSM Time**	**# Sweeps**
1408 × 1408	5.9449e-002	1.4210e-002	2.45	6.41	2.05	12

METHOD	**TIME**	$\mathcal{R}$	ρ	**R**	**AvHR**	**AvS**	**Mon %**
HCM 22 × 22 cells	1.08				1.151	3.971	
HCM 44 × 44 cells	1.10				1.078	3.724	
HCM 88 × 88 cells	1.08				1.040	3.593	
HCM 176 × 176 cells	1.10				1.020	3.518	
HCM 352 × 352 cells	1.24				1.015	3.496	
HCM 704 × 704 cells	1.63				1.008	3.468	
FHCM 22 × 22 cells	0.79	1.0460	1.0000	1.0000	1.151	1.618	85.5
FHCM 44 × 44 cells	0.74	1.0191	1.0000	1.0000	1.078	1.310	92.6
FHCM 88 × 88 cells	0.74	1.0085	1.0000	1.0000	1.040	1.156	96.2
FHCM 176 × 176 cells	0.78	1.0073	1.0000	1.0000	1.020	1.080	98.4
FHCM 352 × 352 cells	0.95	1.0002	1.0000	1.0000	1.015	1.049	99.3
FHCM 704 × 704 cells	1.41	1.0000	1.0000	1.0000	1.008	1.022	100.0
FMSM 22 × 22 cells	0.58	1.1659	1.0000	1.0000		1.436	
FMSM 44 × 44 cells	0.54	1.0706	1.0000	1.0018		1.218	
FMSM 88 × 88 cells	0.53	1.0821	1.0000	1.0018		1.110	
FMSM 176 × 176 cells	0.57	1.0468	1.0000	1.0008		1.055	
FMSM 352 × 352 cells	0.71	1.0378	1.0000	1.0004		1.028	
FMSM 704 × 704 cells	1.24	1.0064	1.0000	1.0001		1.014	

We note that even the slowest of the HCM trials outperforms FMM, FSM, and LSM on this example. Despite the special alignment of cell boundaries, this example is typical in the following ways:

1. In both Heap-Cell algorithms, as the number of cells increases, the average number of heap removals per cell decreases.

2. In FHCM the average number of sweeps per cell decreases to 1 as h^c decreases.

3. In FHCM the percentage of monotonicity check successes increases as h^c decreases.

4. For timing performance in both HCM and FHCM, the optimal choice of h^c is somewhere in the middle of the tested range.

The reason for #2 is that, as the number of cells J increases, most cells will pass the Monotonicity Check. When the monotonicity percentage is high and each cell has on average 2 "upwinding" neighboring cells, each cell on the heap will have one sweeping direction tagged. This observation combined with #1 explains #2.

Combining #1 and #2 and the fact that the length of the heap also increases with J there is a complexity trade-off that explains #4. As J tends to M, the complexity of both Heap-Cell algorithms is similar to that of Fast Marching. As J tends to 1, the complexity of HCM is similar to that of Locking Sweeping.

In the second example we use 8 barriers and the boundaries of the cells are **not aligned** with the discontinuities of the speed function. This example was chosen specifically because it is difficult for our new hybrid methods when using the same cell-decompositions as in the previous example. The performance data is summarized in Table 4.2.

Table 4.2
Performance/convergence results for an 8 wall comb maze example.

Grid Size	L_∞ Error	L_1 Error	FMM Time	FSM Time	LSM Time	# Sweeps
1408 × 1408	6.5644e-002	1.6865e-002	2.50	11.1	3.20	20

METHOD	TIME	$\mathcal{R}$	ρ	R	AvHR	AvS	Mon %
HCM 22 × 22 cells	2.13				2.795	9.293	
HCM 44 × 44 cells	7.68				8.738	28.046	
HCM 88 × 88 cells	6.68				6.798	22.804	
HCM 176 × 176 cells	5.86				5.655	18.872	
HCM 352 × 352 cells	2.95				2.456	8.314	
HCM 704 × 704 cells	1.74				1.037	3.587	
FHCM 22 × 22 cells	1.75	1.4247	1.0000	1.0000	2.946	4.087	84.7
FHCM 44 × 44 cells	5.86	1.4250	1.0000	1.0000	8.991	10.209	94.0
FHCM 88 × 88 cells	4.54	1.3083	1.0000	1.0000	6.976	7.329	98.1
FHCM 176 × 176 cells	3.96	1.2633	1.0000	1.0000	5.754	5.910	99.1
FHCM 352 × 352 cells	2.13	1.8922	1.0000	1.0000	2.468	2.549	99.1
FHCM 704 × 704 cells	1.48	1.5700	1.0000	1.0000	1.037	1.066	100.0
FMSM 22 × 22 cells	0.68	604.49	6.6555	21.036		1.783	
FMSM 44 × 44 cells	0.59	228.29	3.1529	19.442		1.385	
FMSM 88 × 88 cells	0.56	313.01	2.7666	6.4608		1.195	
FMSM 176 × 176 cells	0.58	381.98	1.7374	5.5944		1.097	
FMSM 352 × 352 cells	0.74	45.397	1.1718	2.0506		1.049	
FMSM 704 × 704 cells	1.26	23.303	1.1738	1.3536		1.024	

Notice that since the edges of cells do not coincide with the edges of barriers, the performance of the hybrid methods is not as good as in the previous 4-barrier case, where the edges do coincide. In this example the cells that contain a discontinuity of the speed function may not receive an accurate cell value (for either the Heap-Cell algorithms or FMSM) and may often have poor choices of planned sweeping directions (for FHCM & FMSM). For FHCM, since the error is small in most trials, this effect appears to be rectified at the expense of the same cells being added to the heap many times. For FMSM, since each cell is processed only once, large error remains. The non-monotonic behavior of $\mathcal{R}$ in FMSM and FHCM appears to be due to changes in positions of cell centers relative to barrier edges as h^c decreases.

These comb maze examples illustrate the importance of choosing cell placement and cell sizes so that the speed is roughly constant in each cell. This is necessary both for a small number of sweeps to be effective and for choosing cell values accurately.

4.2. Checkerboards. We return to the checkerboard example already described in section 3.1. For both the 11×11 and 41×41 checkerboard speed functions the center checker is slow. The speed is 1 in the slow checkers and 2 in the fast checkers. The exit set is the single point $Q = \{(0.5, 0.5)\}$.

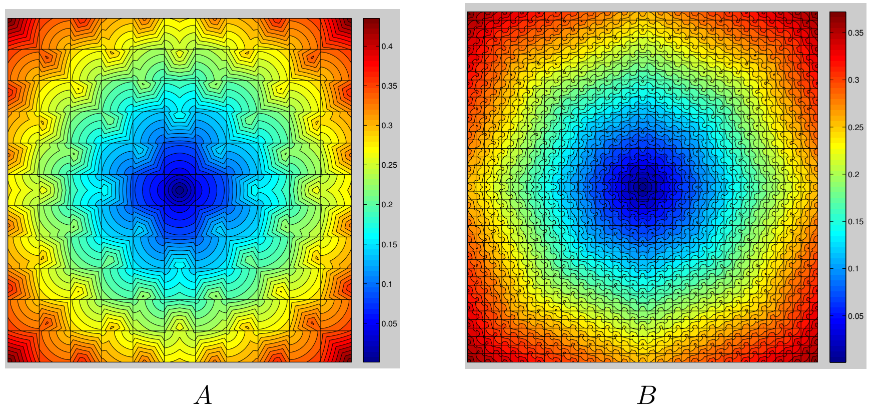

Fig. 4.2. *Min time to the center on checkerboard domains:* 11×11 *checkers (A), and* 41×41 *checkers (B).*

Remark 4.2. Such checkerboard examples arise naturally in the context of front propagation through composite medium, consisting of a periodic mix of isotropic constituent materials with different speed function F. The idea of *homogenization* is to derive a homogeneous but anisotropic speed function $\overline{F}(\boldsymbol{n})$, describing the large-scale properties of the composite material. After $\overline{F}(\boldsymbol{n})$ is computed, the boundary value problems can be solved on a coarser grid. A new efficient method for this homogenization was introduced in [32], using FMM on the fine scale grid since the characteristics are highly oscillatory and the original implementation of sweeping was inefficient. The same test problems were later attacked in [31] using a version of FSM with gridpoint locking (see Remark 2.4). The results in Table 4.4 shows that even the Locking-Sweeping Method becomes significantly less efficient than FMM with the increase in the number of checkers.

Table 4.3
Performance/convergence results for 11×11 *checkerboard example.*

Grid Size	L_∞ **Error**	L_1 **Error**	**FMM Time**	**FSM Time**	**LSM Time**	**# Sweeps**
1408×1408	3.2639e-003	1.7738e-003	3.44	12.3	2.28	16

METHOD	**TIME**	$\mathcal{R}$	ρ	**R**	**AvHR**	**AvS**	**Mon %**
HCM 22×22 cells	1.84				1.397	5.254	
HCM 44×44 cells	1.73				1.209	4.613	
HCM 88×88 cells	1.69				1.083	4.117	
HCM 176×176 cells	1.72				1.029	3.864	
HCM 352×352 cells	1.87				1.009	3.768	
HCM 704×704 cells	2.51				1.003	3.746	
FHCM 22×22 cells	1.17	1.0122	1.0000	1.0000	1.399	1.779	86.3
FHCM 44×44 cells	1.11	1.0208	1.0000	1.0000	1.227	1.535	90.6
FHCM 88×88 cells	1.08	1.0111	1.0000	1.0000	1.091	1.247	95.1
FHCM 176×176 cells	1.14	1.0050	1.0000	1.0000	1.029	1.103	97.8
FHCM 352×352 cells	1.33	1.0006	1.0000	1.0000	1.009	1.043	99.4
FHCM 704×704 cells	2.08	1.0000	1.0000	1.0000	1.003	1.020	100.0
FMSM 22×22 cells	0.87	40.312	1.5725	13.016		1.269	
FMSM 44×44 cells	0.91	18.167	1.0875	7.4581		1.334	
FMSM 88×88 cells	0.89	7.6692	1.0113	3.1400		1.222	
FMSM 176×176 cells	0.91	5.4947	1.0025	2.4813		1.127	
FMSM 352×352 cells	1.07	2.4557	1.0004	1.3888		1.067	
FMSM 704×704 cells	1.84	1.5267	1.0000	1.0032		1.035	

In both examples the cell sizes were chosen to align with the edges of the checkers (i.e., the discontinuities of the speed function). On the 11×11 checkerboard, almost all of the HCM trials

Table 4.4
Performance/convergence results for 41×41 *checkerboard example.*

Grid Size	L_∞ **Error**	L_1 **Error**	**FMM Time**	**FSM Time**	**LSM Time**	**# Sweeps**
1312×1312	1.2452e-002	6.6827e-003	4.13	58.9	11.7	45

METHOD	**TIME**	$\mathcal{R}$	ρ	**R**	**AvHR**	**AvS**	**Mon %**
HCM 41×41 cells	4.18				3.261	11.926	
HCM 82×82 cells	3.05				1.571	5.939	
HCM 164×164 cells	2.84				1.314	4.831	
HCM 328×328 cells	2.81				1.080	3.972	
HCM 656×656 cells	3.36				1.026	3.768	
FHCM 41×41 cells	2.83	1.7506	1.0041	1.7123	3.261	4.600	75.5
FHCM 82×82 cells	2.09	1.0299	1.0006	1.0128	1.584	2.147	78.8
FHCM 164×164 cells	1.95	1.0103	1.0001	1.0000	1.321	1.670	90.4
FHCM 328×328 cells	2.01	1.0173	1.0000	1.0000	1.080	1.236	96.9
FHCM 656×656 cells	2.79	1.0075	1.0000	1.0000	1.026	1.106	100.0
FMSM 41×41 cells	1.46	12.398	3.4110	3.3991		1.164	
FMSM 82×82 cells	1.54	10.551	1.0975	1.7662		1.211	
FMSM 164×164 cells	1.70	4.7036	1.0142	1.7123		1.281	
FMSM 328×328 cells	1.88	2.0192	1.0020	1.7123		1.242	
FMSM 656×656 cells	2.65	1.7506	1.0004	1.7123		1.147	

outperforms FMM and LSM, and most of the FHCM trials are more than twice as fast as LSM and three times faster than FMM while the additional errors are negligible; see Table 4.3.

The 41×41 example is much more difficult for the sweeping algorithms because the number of times the characteristics changes direction increases with the number of checkers. We note that the performance of FMM is only moderately worse here (mostly due to a larger length of level curves and the resulting growth of the "Considered List"). Again, almost all hybrid methods outperform all other methods. The difference is less striking than in the 11×11 example when compared with FMM, but FHCM and FMSM are 4 to 6 times faster than LSM; see Table 4.4.

4.3. Continuous speed functions with a point source. Suppose the speed function is $F \equiv 1$ and the exit set consists of a single point $Q = \{(0.5,\, 0.5)\}$. In this case the viscosity solution is simply the distance to the center of the unit square. We also note that the causal ordering of cells is clearly available here; as a result, FHCM and FMSM do not introduce any additional errors. The performance data is summarized in Table 4.5. For constant speed functions LSM performs significantly better than FMM on fine meshes (such as this one). The reason why FMSM and FHCM are faster than LSM in some trials is that LSM checks all parts of the domain in each sweep, including non-downwinding or already-computed parts. Additionally LSM must perform a final sweep to check that all gridpoints are locked. All of the hybrid algorithms slow down monotonically as J increases because of the cost of sorting the heap.

Table 4.5
Performance/convergence results for constant speed function.

Grid Size	**L_∞ Error**	**L_1 Error**	**FMM Time**	**FSM Time**	**LSM Time**	**# Sweeps**
1408 × 1408	1.0956e-003	6.8382e-004	2.72	2.07	0.83	5

METHOD	**TIME**	**$\mathcal{R}$**	**ρ**	**R**	**AvHR**	**AvS**	**Mon %**
HCM 22 × 22 cells	1.05				1.000	3.692	
HCM 44 × 44 cells	1.12				1.000	3.718	
HCM 88 × 88 cells	1.10				1.000	3.733	
HCM 176 × 176 cells	1.14				1.000	3.742	
HCM 352 × 352 cells	1.29				1.000	3.746	
HCM 704 × 704 cells	1.76				1.000	3.748	
FHCM 22 × 22 cells	0.66	1.0000	1.0000	1.0000	1.000	1.025	100.0
FHCM 44 × 44 cells	0.67	1.0000	1.0000	1.0000	1.000	1.006	100.0
FHCM 88 × 88 cells	0.69	1.0000	1.0000	1.0000	1.000	1.002	100.0
FHCM 176 × 176 cells	0.75	1.0000	1.0000	1.0000	1.000	1.000	100.0
FHCM 352 × 352 cells	0.92	1.0000	1.0000	1.0000	1.000	1.000	100.0
FHCM 704 × 704 cells	1.47	1.0000	1.0000	1.0000	1.000	1.000	100.0
FMSM 22 × 22 cells	0.47	1.0000	1.0000	1.0000		1.103	
FMSM 44 × 44 cells	0.47	1.0000	1.0000	1.0000		1.049	
FMSM 88 × 88 cells	0.49	1.0000	1.0000	1.0000		1.024	
FMSM 176 × 176 cells	0.53	1.0000	1.0000	1.0000		1.012	
FMSM 352 × 352 cells	0.67	1.0000	1.0000	1.0000		1.006	
FMSM 704 × 704 cells	1.23	1.0000	1.0000	1.0000		1.003	

Next we consider examples of min-time to the center under two different oscillatory continuous speed functions. For $F(x,y) = 1 + \frac{1}{2}\sin(20\pi x)\sin(20\pi y)$ the level sets of the value function are shown in Figure 4.3A and the performance data is summarized in Table 4.6. For $F(x,y) = 1 + 0.99\sin(2\pi x)\sin(2\pi y)$ the level sets of the value function are shown in Figure 4.3B and the performance data is summarized in Table 4.7.

Note that HCM outperforms Fast Marching on all trials, and outperforms the sweeping methods significantly on the first example (Table 4.6) despite the fact that no special selection of cell boundaries was made. Small changes in the frequency of the speed function did not significantly alter the performance of the hybrid algorithms. In the second example (Table 4.7) most HCM trials were again faster than LSM and FMM. Note that for some cell sizes, both FMSM and FHCM have $R \ll \mathcal{R} = \max_j(E_j/e_j)$. Whenever R is close to 1, the rate of convergence of hybrid methods (based on L_∞ errors) is the same as that of FMM and FSM.

4.4. Performance on coarser grids. Our hybrid methods exploit the fact that there exists h^c small enough so that most cell-boundaries will be either fully inflow or fully outflow and most pairs of cells will not be mutually dependent. But if the original grid X is sufficiently coarse, this may not be possible to achieve since we also need $h^c \geq 2h$ (otherwise FMM is clearly more efficient). In this subsection we return to some of the previous examples but on significantly coarser grids, to test whether the hybrid methods remain competitive with FMM and LSM. The performance data is summarized in Tables 4.8-4.11; to improve the accuracy of timing on coarser grids, all CPU times are reported for 20 executions of each algorithm.

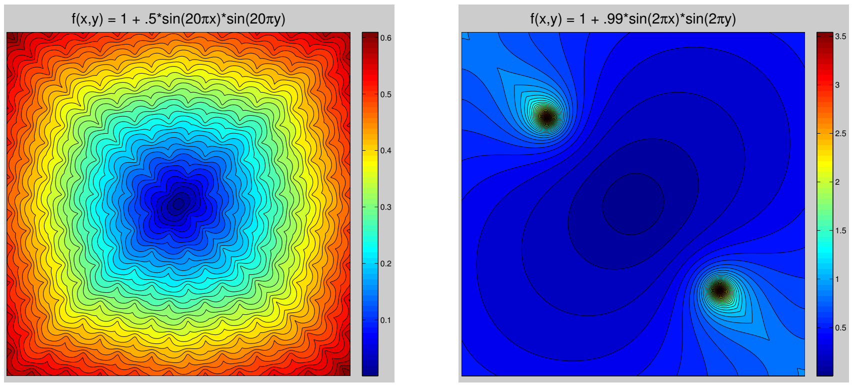

A B

FIG. 4.3. *Min time to the center under sinusoidal speed functions.*

TABLE 4.6
Performance/convergence results for $F(x,y) = 1 + \frac{1}{2}\sin(20\pi x)\sin(20\pi y)$.

Grid Size	L_∞ **Error**	L_1 **Error**	**FMM Time**	**FSM Time**	**LSM Time**	**# Sweeps**
1408 × 1408	4.7569e-003	1.9724e-003	3.74	23.7	6.39	24

METHOD	**TIME**	$\mathcal{R}$	ρ	**R**	**AvHR**	**AvS**	**Mon %**
HCM 22 × 22 cells	3.61				1.913	10.785	
HCM 44 × 44 cells	2.97				1.446	6.811	
HCM 88 × 88 cells	2.60				1.245	5.201	
HCM 176 × 176 cells	2.40				1.117	4.350	
HCM 352 × 352 cells	2.40				1.047	3.945	
HCM 704 × 704 cells	2.92				1.016	3.788	
FHCM 22 × 22 cells	2.72	5.6062	1.1358	2.0960	4.413	5.310	67.3
FHCM 44 × 44 cells	1.82	3.1094	1.1480	1.0000	1.555	2.132	78.7
FHCM 88 × 88 cells	1.61	1.4025	1.0122	1.0000	1.277	1.575	88.2
FHCM 176 × 176 cells	1.53	1.0560	1.0022	1.0000	1.125	1.262	94.5
FHCM 352 × 352 cells	1.65	1.0226	1.0004	1.0000	1.048	1.106	98.1
FHCM 704 × 704 cells	2.40	1.0037	1.0001	1.0000	1.016	1.035	100.0
FMSM 22 × 22 cells	1.14	10.497	2.4811	2.9653		1.262	
FMSM 44 × 44 cells	1.10	6.0892	1.3657	2.2889		1.200	
FMSM 88 × 88 cells	1.16	4.6801	1.0515	1.9504		1.213	
FMSM 176 × 176 cells	1.18	3.4828	1.0074	1.3705		1.126	
FMSM 352 × 352 cells	1.34	1.5987	1.0007	1.0000		1.067	
FMSM 704 × 704 cells	2.14	1.1262	1.0001	1.0000		1.035	

Since M is much smaller here, the $\log M$ term in the complexity of Fast Marching plays less of a role. On most of the examples in this subsection, HCM and FHCM are not much faster than Fast Marching or Locking Sweeping. For example, in Table 4.9 even though the cell boundaries are perfectly aligned with the checker boundaries, both Heap-Cell methods are merely on par with Fast Marching. Note that when h is sufficiently small, their advantage over FMM and LSM is clear (see Table 4.4). FMSM, however, is about twice as fast as the faster of FMM and LSM. In addition, FMSM's error ratios (R, $\mathcal{R}$, and ρ) are smaller here than for the same examples on finer grids in subsections 4.2-4.3.

REMARK 4.3. Since two of the hybrid methods introduce additional errors, an important question is, "Given the total errors resulting from FHCM and FMSM at a given resolution (h, h^c), for which $\bar{h} > h$ would FMM commit similar errors, and how well would FMM perform on that new coarser grid?" For simplicity, assume in the following discussion that the CPU time required by FMM is roughly linear in $M = O(h^{-2})$ and that the resulting L_∞ error is $O(h)$. These are reasonable

TABLE 4.7

Performance/convergence results for $F(x, y) = 1 + 0.99 \sin(2\pi x) \sin(2\pi y)$.

Grid Size	L_∞ **Error**	L_1 **Error**	**FMM Time**	**FSM Time**	**LSM Time**	**# Sweeps**
1408 × 1408	2.1793e-002	9.8506e-004	3.69	12.7	2.73	13

METHOD	**TIME**	$\boldsymbol{\mathcal{R}}$	$\boldsymbol{\rho}$	**R**	**AvHR**	**AvS**	**Mon %**
HCM 22 × 22 cells	2.29				1.165	4.651	
HCM 44 × 44 cells	2.15				1.070	4.132	
HCM 88 × 88 cells	2.11				1.034	3.920	
HCM 176 × 176 cells	2.13				1.015	3.811	
HCM 352 × 352 cells	2.26				1.008	3.763	
HCM 704 × 704 cells	2.80				1.002	3.741	
FHCM 22 × 22 cells	1.37	60.848	1.0020	1.0014	1.174	1.409	92.7
FHCM 44 × 44 cells	1.28	4.5786	1.0002	1.0001	1.078	1.185	96.1
FHCM 88 × 88 cells	1.28	1.0224	1.0000	1.0000	1.039	1.086	98.2
FHCM 176 × 176 cells	1.35	1.0019	1.0000	1.0000	1.017	1.039	99.3
FHCM 352 × 352 cells	1.55	1.0003	1.0000	1.0000	1.008	1.018	99.7
FHCM 704 × 704 cells	2.27	1.0001	1.0000	1.0000	1.002	1.006	100.0
FMSM 22 × 22 cells	1.13	1362.4	1.0270	1.0053		1.231	
FMSM 44 × 44 cells	1.06	174.62	1.0054	1.0053		1.116	
FMSM 88 × 88 cells	1.05	38.545	1.0021	1.0046		1.057	
FMSM 176 × 176 cells	1.09	7.1581	1.0006	1.0046		1.029	
FMSM 352 × 352 cells	1.28	1.1687	1.0001	1.0028		1.014	
FMSM 704 × 704 cells	2.08	1.0724	1.0000	1.0000		1.007	

assumptions for coarse grids; e.g., see Tables 4.8-4.11. For example, if we want to decrease time by a factor of p^2, then $M \to M/p^2$, $h \to p * h$ (in 2-d), and errors would increase by a factor of p. Such estimates allow for a more accurate performance comparison between FMM and FMSM (or FHCM) based on the ratio $\mathbf{R}$. Dividing the reported FMM time by the value $\mathbf{R}^2$, we will arrive at an estimate for the new FMM time computed on a coarser $\bar{h}$-grid with errors similar to those committed by FMSM on an(h,h^c)-grid.

Among Tables 4.8-4.11, the overall worst-case scenario for FMSM under this analysis is the 11×11 checkerboard example. Using the data in Table 4.8 with $M = 176^2$ and comparing FMM with FMSM at 22^2, 44^2, and 88^2 cells, the new estimated FMM times would be $0.82/(2.392^2) = .343$, $0.82/(1.3489^2) = .608$, and $0.82/(1.004^2) = .817$. Comparing this to 0.29, 0.35, 0.53 reported for FMSM, we see that each of the cell trials still outperforms the corresponding improved time of FMM. Similar conclusions are reached when this analysis is performed using error ratios in L_1 norms.

Table 4.8

Performance/convergence results for 20 trials of 11×11 *checkerboard example on a coarse grid.*

Grid Size	L_∞ **Error**	L_1 **Error**	**FMM Time**	**FSM Time**	**LSM Time**	**# Sweeps**
176 × 176	2.0986e-002	1.1087e-002	0.82	3.91	0.81	16

METHOD	**TIME**	$\mathcal{R}$	ρ	**R**	**AvHR**	**AvS**	**Mon %**
HCM 22 × 22 cells	0.59				1.438	5.134	
HCM 44 × 44 cells	0.59				1.171	4.199	
HCM 88 × 88 cells	0.72				1.041	3.779	
FHCM 22 × 22 cells	0.41	1.0017	1.0000	1.0000	1.440	1.804	88.2
FHCM 44 × 44 cells	0.43	1.0015	1.0000	1.0000	1.171	1.374	97.0
FHCM 88 × 88 cells	0.59	1.0000	1.0000	1.0000	1.041	1.158	100.0
FMSM 22 × 22 cells	0.29	5.1670	1.0770	2.3920		1.269	
FMSM 44 × 44 cells	0.35	2.2742	1.0066	1.3489		1.334	
FMSM 88 × 88 cells	0.53	1.2309	1.0004	1.0040		1.221	

Grid Size	L_∞ **Error**	L_1 **Error**	**FMM Time**	**FSM Time**	**LSM Time**	**# Sweeps**
352 × 352	1.1470e-002	6.0787e-003	3.52	15.4	3.16	16

METHOD	**TIME**	$\mathcal{R}$	ρ	**R**	**AvHR**	**AvS**	**Mon %**
HCM 22 × 22 cells	2.40				1.438	5.302	
HCM 44 × 44 cells	2.25				1.208	4.465	
HCM 88 × 88 cells	2.32				1.059	3.904	
HCM 176 × 176 cells	2.91				1.018	3.757	
FHCM 22 × 22 cells	1.61	1.1194	1.0002	1.0725	1.490	1.936	84.9
FHCM 44 × 44 cells	1.53	1.0434	1.0000	1.0000	1.228	1.508	92.2
FHCM 88 × 88 cells	1.69	1.0745	1.0000	1.0000	1.059	1.190	97.5
FHCM 176 × 176 cells	2.40	1.0273	1.0000	1.0000	1.018	1.086	100.0
FMSM 22 × 22 cells	1.12	10.551	1.1593	4.0315		1.269	
FMSM 44 × 44 cells	1.21	4.7036	1.0252	3.9089		1.334	
FMSM 88 × 88 cells	1.38	4.1945	1.0093	3.9089		1.222	
FMSM 176 × 176 cells	2.12	4.1945	1.0074	3.9089		1.127	

Table 4.9

Performance/convergence results for 20 trials of 41×41 *checkerboard on a coarse grid.*

Grid Size	L_∞ **Error**	L_1 **Error**	**FMM Time**	**FSM Time**	**LSM Time**	**# Sweeps**
164 × 164	7.1112e-002	3.8397e-002	1.08	17.9	4.01	44

METHOD	**TIME**	$\mathcal{R}$	ρ	**R**	**AvHR**	**AvS**	**Mon %**
HCM 41 × 41 cells	1.13				2.204	7.041	
HCM 82 × 82 cells	1.05				1.261	4.215	
FHCM 41 × 41 cells	0.85	1.0000	1.0000	1.0000	2.204	2.449	92.2
FHCM 82 × 82 cells	0.90	1.0000	1.0000	1.0000	1.261	1.474	100.0
FMSM 41 × 41 cells	0.53	1.4878	1.0850	1.0197		1.163	
FMSM 82 × 82 cells	0.77	1.1277	1.0162	1.0193		1.210	

Grid Size	L_∞ **Error**	L_1 **Error**	**FMM Time**	**FSM Time**	**LSM Time**	**# Sweeps**
328 × 328	4.0403e-002	2.3205e-002	4.44	73.3	16.6	45

METHOD	**TIME**	$\mathcal{R}$	ρ	**R**	**AvHR**	**AvS**	**Mon %**
HCM 41 × 41 cells	5.42				2.873	9.970	
HCM 82 × 82 cells	4.02				1.500	5.104	
HCM 164 × 164 cells	4.19				1.181	4.105	
FHCM 41 × 41 cells	3.65	1.0988	1.0008	1.0679	2.873	3.802	81.6
FHCM 82 × 82 cells	2.90	1.0236	1.0000	1.0000	1.501	1.923	88.0
FHCM 164 × 164 cells	3.55	1.0000	1.0000	1.0000	1.181	1.384	100.0
FMSM 41 × 41 cells	1.88	2.9459	1.4364	1.4668		1.164	
FMSM 82 × 82 cells	2.22	2.3040	1.0533	1.1457		1.211	
FMSM 164 × 164 cells	3.27	1.1540	1.0009	1.0679		1.281	

Table 4.10

Performance/convergence results for 20 trials of $F(x,y) = 1 + \frac{1}{2}\sin(20\pi x)\sin(20\pi y)$ on a coarse grid.

Grid Size	**L_∞ Error**	**L_1 Error**	**FMM Time**	**FSM Time**	**LSM Time**	**# Sweeps**
176 × 176	3.6535e-002	1.3374e-002	0.94	8.77	3.08	28

METHOD	**TIME**	**$\mathcal{R}$**	**ρ**	**R**	**AvHR**	**AvS**	**Mon %**
HCM 22 × 22 cells	0.97				1.773	8.233	
HCM 44 × 44 cells	0.88				1.280	4.992	
HCM 88 × 88 cells	0.87				1.100	3.975	
FHCM 22 × 22 cells	0.66	1.3736	1.0209	1.0000	2.153	2.814	69.3
FHCM 44 × 44 cells	0.60	1.1703	1.0186	1.0000	1.285	1.684	87.7
FHCM 88 × 88 cells	0.71	1.1170	1.0072	1.0000	1.100	1.234	100.0
FMSM 22 × 22 cells	0.38	7.0809	1.2945	1.0359		1.244	
FMSM 44 × 44 cells	0.42	2.2023	1.0402	1.0100		1.197	
FMSM 88 × 88 cells	0.64	1.0945	1.0024	1.0000		1.213	

Grid Size	**L_∞ Error**	**L_1 Error**	**FMM Time**	**FSM Time**	**LSM Time**	**# Sweeps**
352 × 352	1.8414e-002	7.0584e-003	3.92	33.7	11.1	27

METHOD	**TIME**	**$\mathcal{R}$**	**ρ**	**R**	**AvHR**	**AvS**	**Mon %**
HCM 22 × 22 cells	4.43				1.909	9.864	
HCM 44 × 44 cells	3.57				1.403	5.969	
HCM 88 × 88 cells	3.18				1.178	4.493	
HCM 176 × 176 cells	3.45				1.060	3.891	
FHCM 22 × 22 cells	2.89	1.8770	1.0300	1.0202	2.905	3.630	66.2
FHCM 44 × 44 cells	2.29	1.8064	1.0712	1.0000	1.425	1.918	82.2
FHCM 88 × 88 cells	2.23	1.2724	1.0108	1.0000	1.182	1.394	93.7
FHCM 176 × 176 cells	2.84	1.0500	1.0016	1.0000	1.060	1.130	100.0
FMSM 22 × 22 cells	1.44	4.3257	1.4890	1.1939		1.246	
FMSM 44 × 44 cells	1.46	2.2958	1.0975	1.1932		1.197	
FMSM 88 × 88 cells	1.78	1.7082	1.0110	1.0806		1.213	
FMSM 176 × 176 cells	2.57	1.0845	1.0010	1.0000		1.126	

Table 4.11

Performance/convergence results for 20 trials $F(x,y) = 1 + 0.99\sin(2\pi x)\sin(2\pi y)$ on a coarse grid.

Grid Size	**L_∞ Error**	**L_1 Error**	**FMM Time**	**FSM Time**	**LSM Time**	**# Sweeps**
176 × 176	1.0533e-001	5.6430e-003	0.93	4.00	0.93	13

METHOD	**TIME**	**$\mathcal{R}$**	**ρ**	**R**	**AvHR**	**AvS**	**Mon %**
HCM 22 × 22 cells	0.74				1.165	4.496	
HCM 44 × 44 cells	0.73				1.085	4.040	
HCM 88 × 88 cells	0.83				1.026	3.790	
FHCM 22 × 22 cells	0.47	1.0952	1.0020	1.0004	1.169	1.388	94.2
FHCM 44 × 44 cells	0.50	1.0200	1.0005	1.0000	1.087	1.173	97.9
FHCM 88 × 88 cells	0.66	1.0045	1.0001	1.0000	1.027	1.051	100.0
FMSM 22 × 22 cells	0.37	1.2819	1.0044	1.0164		1.231	
FMSM 44 × 44 cells	0.41	1.1839	1.0007	1.0053		1.116	
FMSM 88 × 88 cells	0.59	1.0979	1.0001	1.0000		1.057	

Grid Size	**L_∞ Error**	**L_1 Error**	**FMM Time**	**FSM Time**	**LSM Time**	**# Sweeps**
352 × 352	6.8813e-002	3.1818e-003	3.84	15.9	3.64	13

METHOD	**TIME**	**$\mathcal{R}$**	**ρ**	**R**	**AvHR**	**AvS**	**Mon %**
HCM 22 × 22 cells	3.00				1.178	4.624	
HCM 44 × 44 cells	2.76				1.076	4.082	
HCM 88 × 88 cells	2.83				1.033	3.853	
HCM 176 × 176 cells	3.29				1.008	3.747	
FHCM 22 × 22 cells	1.82	1.1364	1.0040	1.0004	1.178	1.405	93.2
FHCM 44 × 44 cells	1.71	1.0204	1.0005	1.0000	1.080	1.170	97.7
FHCM 88 × 88 cells	1.98	1.0034	1.0001	1.0000	1.034	1.071	99.2
FHCM 176 × 176 cells	2.69	1.0006	1.0000	1.0000	1.008	1.022	100.0
FMSM 22 × 22 cells	1.44	2.3482	1.0080	1.0074		1.231	
FMSM 44 × 44 cells	1.42	1.5167	1.0014	1.0037		1.116	
FMSM 88 × 88 cells	1.61	1.1989	1.0004	1.0034		1.057	
FMSM 176 × 176 cells	2.44	1.0953	1.0001	1.0015		1.028	

Remark 4.4. We could perform a similar comparison between FMSM and sweeping methods, but the latter allow for yet another speed up technique: the sweeping can be stopped before the full convergence to the solution of system (2.1). In fact, in many implementations of Fast Sweeping, the method terminates when the changes in grid values due to the most recent sweep fall below some positive threshold t^*; e.g., see [26]. Similarly to FHCM and FMSM, this results in additional errors, and it is useful to consider both these errors and the corresponding savings in computational time. To the best of our knowledge, this issue has not been analyzed so far. The practical implementations of FSM and LSM typically select t^* heuristically or make it proportional to the grid-size h. It is usually claimed that the number of sweeps necessary for convergence is h-independent [44, 51]. Tables 4.9 and 4.10 show that the number of sweeps-to-convergence (i.e., for $t^* = 0$) may in fact depend on h. We believe that Figure 2.1 provides one possible explanation for this phenomenon (since the location of gridpoints relative to shocklines is h-dependent).

For $t^* > 0$, the more relevant questions are:

1. How well do the changes in the most recent sweep represent the additional errors, which would result if we were to stop the sweeping?
2. Is the number of sweeps (needed for a fixed $t^* > 0$) really h-independent?
3. Supposing the additional ("early-termination") errors could be estimated, would the number of required sweeps be h-independent?
4. Supposing FSM or LSM were run for as many sweeps as necessary to make the additional errors approximately the same as those introduced by FMSM or FHCM, would the resulting computational costs be less than those of hybrid methods?

To answer these questions for one specific (41×41 checkerboard) example, we have run both sweeping methods on 164^2 and 1312^2 grids. In table 4.12 we report the L_∞ change in grid values, the percentage of gridpoints changing, and potential early-termination errors ($\boldsymbol{\mathcal{R}}$, $\boldsymbol{\rho}$, and $\mathbf{R}$) after each sweep. At least for this particular example:

1. The answer to Question 1 is inconclusive, though the max changes are clearly correlated with $\mathbf{R}$ and ρ.
2. The answer to Question 2 is negative; moreover, after the same number of sweeps, the max changes on the 1312^2 grid are clearly larger than on the 164^2 grid.
3. The answer to Question 3 is negative; e.g., $\mathbf{R}$ reduces below 1.1 after only 12 sweeps on the 164^2 grid, but the same reduction on the 1312^2 grid requires 42 sweeps.
4. To answer the last question, we note that for this example FHCM produces very small additional errors, while FMSM results in $\mathbf{R} = 1.0197$ and $\mathbf{R} = 1.0193$ (on the 164^2 grid with 21^2 and 42^2 cells, respectively; see Table 4.9). As Table 4.12A shows, 16 sweeps would be needed for FSM or LSM to produce the same $\mathbf{R}$ values on this grid. Our computational experiment shows that FSM and LSM times for these 16 sweeps are 6.62 and 2.91 seconds respectively (note that this is the total time for 20 trials, similar to the times reported in Table 4.9). Thus, FMSM is still more than 3.5 times faster than the early-terminated LSM and more than 8 times faster than the early-terminated FSM. For the 1312^2 example, we see that the error ratios take longer to converge to 1 for the sweeping methods (Table 4.12B). The FMSM's $\mathbf{R}$ values of $\{3.3991, 1.7662, 1.7123\}$ (from Table 4.4, for different cell sizes) correspond to $\{28, 37, 37\}$ sweeps in Table 4.12B. The experimentally measured early-terminated execution times for FSM and LSM are $\{36.85, 48.77, 48.77\}$ seconds and $\{7.40, 11.68, 11.68\}$ seconds respectively. Again, FMSM still holds a large advantage (more than 4 times faster than LSM and more than 18 times faster than FSM). We note that for both the 164^2 and 1312^2 cases, the early-terminated FSM time was linear in the number of sweeps, while LSM did not receive as much of a speed boost; this is natural since the percentage of gridpoints changing in the omitted "later iterations" is low, and the LSM's computational cost is largely dependent on the number of unlocked gridpoints in each sweep.

Sweep #	**Max Change**	**% GPs changing**	$\mathcal{R}$	ρ	**R**
1	1.00e+008	26.22	-	-	-
2	1.000e+008	31.856	-	-	-
3	1.000e+008	58.247	44.595	1.7709	4.8179
4	2.7622e-001	44.4527	1.4685	1.1027	1.2445
5	6.3846e-003	41.5341	1.4224	1.0888	1.1995
6	5.9641e-003	41.1957	1.4195	1.0759	1.1995
7	5.9641e-003	41.0730	1.3832	1.0631	1.1951
8	5.4993e-003	40.1919	1.3331	1.0509	1.1562
9	4.9918e-003	37.0650	1.3243	1.0440	1.1205
10	4.9918e-003	36.6337	1.3230	1.0377	1.1205
11	4.9918e-003	36.3995	1.2881	1.0314	1.1191
12	4.7740e-003	34.6743	1.2492	1.0255	1.0854
13	4.5076e-003	31.3318	1.2403	1.0218	1.0532
14	4.5076e-003	30.8150	1.2400	1.0185	1.0520
15	4.5076e-003	30.4767	1.2098	1.0152	1.0511
16	4.1600e-003	28.0934	1.1820	1.0121	1.0270
17	3.6304e-003	22.6502	1.1646	1.0102	1.0004
18	3.6304e-003	21.8062	1.1644	1.0085	1.0000
19	3.6304e-003	21.2374	1.1467	1.0068	1.0000
20	3.2984e-003	19.1404	1.1268	1.0052	1.0000
21	2.7917e-003	14.3367	1.1079	1.0043	1.0000
22	2.7142e-003	13.6340	1.1079	1.0035	1.0000
23	2.7142e-003	13.2250	1.0951	1.0027	1.0000
24	2.4311e-003	11.6746	1.0812	1.0020	1.0000
25	2.1725e-003	8.4659	1.0637	1.0015	1.0000
26	1.8533e-003	7.9677	1.0630	1.0012	1.0000
27	1.8533e-003	7.6852	1.0546	1.0009	1.0000
28	1.7075e-003	6.6664	1.0457	1.0006	1.0000
29	1.5049e-003	4.8000	1.0365	1.0004	1.0000
30	1.1216e-003	4.4653	1.0303	1.0003	1.0000
31	1.1216e-003	4.2646	1.0257	1.0002	1.0000
32	1.0109e-003	3.5656	1.0209	1.0001	1.0000
33	8.5675e-004	2.2754	1.0153	1.0001	1.0000
34	4.8751e-004	2.0300	1.0110	1.0001	1.0000
35	4.8751e-004	1.8813	1.0087	1.0000	1.0000
36	4.2582e-004	1.4314	1.0068	1.0000	1.0000
37	3.4338e-004	0.7064	1.0043	1.0000	1.0000
38	1.1188e-004	0.5689	1.0025	1.0000	1.0000
39	1.1188e-004	0.4871	1.0015	1.0000	1.0000
40	8.9968e-005	0.2863	1.0011	1.0000	1.0000
41	6.8284e-005	0.0632	1.0006	1.0000	1.0000
42	2.4066e-005	0.0297	1.0002	1.0000	1.0000
43	1.0931e-005	0.0112	1.0000	1.0000	1.0000
44	0.0000e+000	0.0000	1.0000	1.0000	1.0000

A

Sweep #	**Max Change**	**% GPs changing**	$\mathcal{R}$	ρ	**R**
1	1.0e+008	25.2	-	-	-
2	1.000e+008	34.249	-	-	-
3	1.000e+008	62.372	48.051	9.2339	30.026
4	3.621e-001	49.221	12.002	4.1935	7.7797
5	1.0709e-002	43.0590	11.194	3.9168	7.7098
6	1.0252e-002	42.1586	10.474	3.6528	7.2822
7	1.0252e-002	42.0001	10.269	3.3925	7.2771
8	1.0229e-002	39.8694	9.6885	3.1431	6.9538
9	1.0207e-002	34.3652	9.6713	2.9458	6.9386
10	1.0207e-002	33.2951	9.4074	2.7562	6.5653
11	1.0207e-002	33.1453	9.0914	2.5686	6.5623
12	1.0185e-002	31.2973	8.6218	2.3892	6.1648
13	1.0165e-002	26.4975	8.5771	2.2483	6.1607
14	1.0165e-002	25.5465	8.3781	2.1135	5.8497
15	1.0165e-002	25.3961	8.0972	1.9804	5.8487
16	1.0145e-002	23.7761	7.5600	1.8536	5.4607
17	1.0127e-002	19.6460	7.5550	1.7561	5.4571
18	1.0127e-002	18.8095	7.2488	1.6635	5.0667
19	1.0127e-002	18.6819	7.0133	1.5722	5.0658
20	1.0108e-002	17.2760	6.5857	1.4861	4.7569
21	1.0092e-002	13.8028	6.5691	1.4221	4.7449
22	1.0092e-002	13.0992	6.2438	1.3619	4.3682
23	1.0092e-002	12.9746	6.0465	1.3027	4.3674
24	1.0075e-002	11.8224	5.5031	1.2475	3.9749
25	1.0060e-002	9.0073	5.4990	1.2088	3.9720
26	1.0060e-002	8.4400	5.2424	1.1730	3.6712
27	1.0060e-002	8.3202	5.0816	1.1380	3.6705
28	1.0045e-002	7.3932	4.5433	1.1059	3.2817
29	1.0031e-002	5.2311	4.5402	1.0854	3.2794
30	1.0031e-002	4.8007	4.1140	1.0670	2.8875
31	1.0031e-002	4.7054	3.9971	1.0491	2.8871
32	1.0018e-002	4.0108	3.5893	1.0334	2.5926
33	1.0005e-002	2.5072	3.5711	1.0249	2.5795
34	1.0005e-002	2.2144	3.1264	1.0177	2.2008
35	1.0005e-002	2.1276	3.0465	1.0109	2.2005
36	9.9928e-003	1.6782	2.4976	1.0053	1.8040
37	9.9809e-003	0.8296	2.4942	1.0034	1.8016
38	9.9809e-003	0.6789	2.1526	1.0020	1.5223
39	9.9809e-003	0.6047	2.1076	1.0009	1.5223
40	9.9619e-003	0.3888	1.5638	1.0002	1.1295
41	5.0711e-003	0.1151	1.5638	1.0001	1.1295
42	4.9343e-003	0.0698	1.1631	1.0000	1.0000
43	1.4668e-003	0.0338	1.0000	1.0000	1.0000
44	0.0000e+000	0.0000	1.0000	1.0000	1.0000

B

TABLE 4.12

Maximum change of V for the sweeping methods for the 41×41 checkerboard example on the 164×164 grid (A) and 1312×1312 grid (B).

4.5. Continuous speed functions with general boundary conditions. Next we return to speed functions $F(x,y) = 1 + 0.99 \sin(2\pi x) \sin(2\pi y)$ and $F(x,y) = 1 + \frac{1}{2} \sin(20\pi x) \sin(20\pi y)$, but this time with zero boundary conditions on the entire boundary of the square. The performance data is summarized in Tables 4.13 and 4.14.

REMARK 4.5. Our current implementation of FMSM treats the coarse gridpoints nearest to the boundary as *Accepted* in the initialization. If there is more than one coarse gridpoint in the exit set, as in the following examples, care must be taken when ranking the "acceptance order" of these coarse gridpoints. While in the case of single-point exit sets it is safe to assign a zero value to these coarse gridpoints, for general boundary conditions we compute the values by a one-sided update from the cell center to the nearest point on the boundary. In addition, our FMSM implementation iterates FSM to convergence on all cells containing parts of Q.

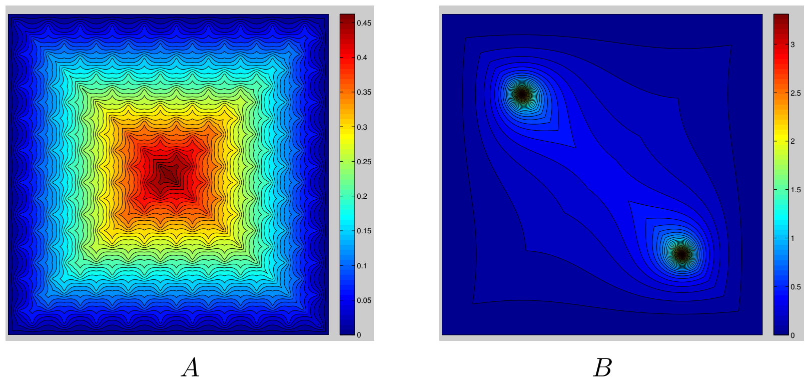

Fig. 4.4. *Min time to $\partial\Omega$ under two sinusoidal speed functions.*

Table 4.13

Performance/convergence results for $F(x,y) = 1 + \frac{1}{2}\sin(20\pi x)\sin(20\pi y)$ with $Q = \partial\Omega$.

Grid Size	**L_∞ Error**	**L_1 Error**	**FMM Time**	**FSM Time**	**LSM Time**	**# Sweeps**
1408 × 1408	1.3670e-003	3.7171e-004	3.89	24.3	6.62	24

METHOD	**TIME**	**$\mathcal{R}$**	**ρ**	**R**	**AvHR**	**AvS**	**Mon %**
HCM 22 × 22 cells	3.48				1.853	10.273	
HCM 44 × 44 cells	2.92				1.470	6.811	
HCM 88 × 88 cells	2.53				1.195	4.987	
HCM 176 × 176 cells	2.35				1.098	4.301	
HCM 352 × 352 cells	2.37				1.046	3.951	
HCM 704 × 704 cells	2.91				1.018	3.785	
FHCM 22 × 22 cells	2.60	20660	1.5321	3.2150	2.915	4.498	54.5
FHCM 44 × 44 cells	1.95	62.164	1.2465	1.5447	1.539	2.502	68.0
FHCM 88 × 88 cells	1.66	64.719	1.0187	1.0128	1.223	1.749	83.9
FHCM 176 × 176 cells	1.55	5.7122	1.0032	1.0063	1.102	1.361	92.4
FHCM 352 × 352 cells	1.66	1.1083	1.0007	1.0011	1.047	1.165	97.5
FHCM 704 × 704 cells	2.40	1.0192	1.0001	1.0001	1.018	1.064	100.0
FMSM 22 × 22 cells	1.97	1.6383e+5	7.8665	12.339		2.184	
FMSM 44 × 44 cells	1.67	1.1325e+6	2.6113	4.2370		1.892	
FMSM 88 × 88 cells	1.42	5506.21	1.0388	1.8072		1.527	
FMSM 176 × 176 cells	1.29	859.45	1.0044	1.2609		1.265	
FMSM 352 × 352 cells	1.40	253.58	1.0009	1.0270		1.134	
FMSM 704 × 704 cells	2.17	6.6107	1.0001	1.0000		1.062	

5. Conclusions.

We have introduced three new efficient hybrid methods for Eikonal equations. Using a splitting of the domain into a number of cells (with the speed function approximately constant on each of them), our methods employ sweeping methods on individual cells with the order of cell-processing and the direction of sweeps determined by a marching-like procedure on a coarser scale. Such techniques may introduce additional errors to attain higher computational efficiency. Of these new methods FMSM is generally the fastest and somewhat easier to implement, while FHCM introduces smaller additional errors, and HCM is usually the slowest of the three but provably converges to the exact solutions. The numerical evidence presented in this paper strongly suggests that

- when h and h^c are sufficiently small, additional errors introduced by FMSM and FHCM are negligible compared to those already present due to discretization;
- for the right (h, h^c)-combinations, our new hybrid algorithms significantly outperform the prior fast methods (FMM, FSM, and LSM).

Table 4.14

Performance/convergence results for $F(x,y) = 1 + 0.99\sin(2\pi x)\sin(2\pi y)$ *with* $Q = \partial\Omega$.

Grid Size	L_∞ **Error**	L_1 **Error**	**FMM Time**	**FSM Time**	**LSM Time**	**# Sweeps**
1408 × 1408	2.2246e-002	2.7572e-004	3.66	8.06	2.58	8

METHOD	**TIME**	$\mathcal{R}$	ρ	**R**	**AvHR**	**AvS**	**Mon %**
HCM 22 × 22 cells	2.03				1.176	4.448	
HCM 44 × 44 cells	1.97				1.089	4.021	
HCM 88 × 88 cells	1.93				1.047	3.830	
HCM 176 × 176 cells	1.96				1.020	3.718	
HCM 352 × 352 cells	2.10				1.009	3.670	
HCM 704 × 704 cells	2.74				1.006	3.649	
FHCM 22 × 22 cells	1.51	136.37	1.0001	1.0000	1.176	1.903	93.4
FHCM 44 × 44 cells	1.35	2.4167	1.0000	1.0000	1.091	1.443	99.0
FHCM 88 × 88 cells	1.32	2.4167	1.0000	1.0000	1.048	1.226	99.6
FHCM 176 × 176 cells	1.39	1.6390	1.0000	1.0000	1.020	1.110	99.8
FHCM 352 × 352 cells	1.57	1.0000	1.0000	1.0000	1.009	1.054	99.9
FHCM 704 × 704 cells	2.33	1.0000	1.0000	1.0000	1.006	1.028	100.0
FMSM 22 × 22 cells	1.57	12592	1.0441	1.0000		1.599	
FMSM 44 × 44 cells	1.27	355.53	1.0088	1.0000		1.306	
FMSM 88 × 88 cells	1.15	355.53	1.0055	1.0000		1.157	
FMSM 176 × 176 cells	1.14	303.61	1.0030	1.0000		1.079	
FMSM 352 × 352 cells	1.31	134.60	1.0012	1.0000		1.040	
FMSM 704 × 704 cells	2.11	68.199	1.0004	1.0000		1.014	

Of course, the rate of change of the speed function F determines the suitable size of cells and our methods are particularly efficient for the examples where F is piecewise constant.

All of the examples considered here used predetermined uniform cell-sizes. From a practitioner's point of view, the value of the proposed methods will greatly increase once we develop bounds and estimates for the additional errors in both FMSM and FHCM. Such estimates would be also very useful for the computational costs of all three hybrid methods on a given cell-decomposition. In the future, we intend to automate the choice of cell-sizes (based on the speed function and user-specified tolerances for additional errors) and further relax the requirement that all cells need to be uniform. A generalization of this approach to cell-subdivision of unstructured meshes will also be valuable.

We expect the extensions of these techniques to higher dimensional problems to be useful for many applications and relatively straight-forward – especially for FMSM and HCM. A higher dimensional version of the "cell boundary monotonicity check" will be needed to extend FHCM.

Other obvious directions for future work include extensions to higher-order accurate discretizations and parallelizable cell-level numerical methods for Eikonal equations.

More generally, we hope that the ideas presented here can serve as a basis for causal domain decomposition and efficient two-scale methods for other static nonlinear PDEs, including those arising in anisotropic optimal control and differential games.

REFERENCES

[1] Ahuja, R.K., Magnanti, T.L., & Orlin, J.B., *Network Flows*, Prentice Hall, Upper Saddle River, NJ, 1993.

[2] K. Alton & I. M. Mitchell, *Fast Marching Methods for Stationary Hamilton-Jacobi Equations with Axis-Aligned Anisotropy*, SIAM J. Numer. Anal., 47:1, pp. 363–385, 2008.

[3] S. Bak, J. McLaughlin, and D. Renzi, *Some improvements for the fast sweeping method*, SIAM J. on Sci. Comp., 32(5), 2010.

[4] M. Bardi & I. Capuzzo Dolcetta, *Optimal Control and Viscosity Solutions of Hamilton-Jacobi-Bellman Equations*, Birkhäuser Boston, 1997.

[5] G. Barles and P. E. Souganidis, *Convergence of approximation schemes for fully nonlinear second order equations*, Asymptot. Anal., 4:271-283, 1991.

[6] Bellman, R., *Dynamic Programming*, Princeton Univ. Press, Princeton, NJ, 1957.

[7] Bertsekas, D. P., *A Simple and Fast Label Correcting Algorithm for Shortest Paths*, Networks, Vol. 23, pp. 703-709, 1993.

[8] Bertsekas, D.P., *Network optimization: continuous & discrete models*, Athena Scientific, Boston, MA, 1998.

[9] Bertsekas, D.P., *Dynamic Programming and Optimal Control*, 2nd Edition, Volumes I and II, Athena Scientific, Boston, MA, 2001.

[10] Bertsekas, D. P., Guerriero, F., and Musmanno, R., *Parallel Asynchronous Label Correcting Methods for Shortest Paths*, J. of Optimization Theory and Applications, Vol. 88, pp. 297-320, 1996.

[11] F. Bornemann and C. Rasch, *Finite-element Discretization of Static Hamilton-Jacobi Equations based on a Local Variational Principle*, Computing and Visualization in Science, 9(2), pp.57-69, 2006.

[12] Boué, M. & Dupuis, P., *Markov chain approximations for deterministic control problems with affine dynamics and quadratic cost in the control*, SIAM J. Numer. Anal., 36:3, pp.667-695, 1999.

[13] M.G. Crandall, L.C. Evans, & P-L.Lions, *Some Properties of Viscosity Solutions of Hamilton-Jacobi Equations*, Tran. AMS, 282 (1984), pp. 487–502.

[14] Crandall, M.G. & Lions, P-L., *Viscosity Solutions of Hamilton-Jacobi Equations*, Tran. AMS, 277, pp. 1-43, 1983.

[15] E. Cristiani and M. Falcone, *A Characteristics Driven Fast Marching Method for the Eikonal Equation*, in “Numerical Mathematics and Advanced Applications”, pp. 695-702, Proceedings of ENUMATH 2007, Graz, Austria, September 2007.

[16] Danielsson, P.-E., *Euclidean Distance Mapping*, Computer Graphics and Image Processing, 14, pp.227–248, 1980.

[17] R. Dial, *Algorithm 360: Shortest path forest with topological ordering*, Comm. ACM, pp. 632–633, 1969.

[18] E.W. Dijkstra, *A Note on Two Problems in Connection with Graphs*, Numerische Mathematik, 1 (1959), pp. 269–271.

[19] M. Falcone, *The Minimum Time Problem and Its Applications to Front Propagation*, in “Motion by Mean Curvature and Related Topics”, Proceedings of the International Conference at Trento, 1992, Walter de Gruyter, New York, 1994.

[20] Glover, F., Glover, R., and Klingman, D., *The Threshold Shortest Path Algorithm*, Math. Programming Studies, Vol. 26, pp. 12-37, 1986.

[21] Gonzales, R. & Rofman, E., *On Deterministic Control Problems: an Approximate Procedure for the Optimal Cost, I, the Stationary Problem*, SIAM J. Control Optim., 23, 2, pp. 242-266, 1985.

[22] Gremaud, P.A. & Kuster, C.M., *Computational Study of Fast Methods for the Eikonal Equation*, SIAM J. Sc. Comp., 27, pp.1803-1816, 2006.

[23] S.-R. Hysing and S. Turek, *The Eikonal equation: Numerical efficiency vs. algorithmic complexity on quadrilateral grids*, In Proceedings of Algoritmy 2005, pp.22-31, 2005.

[24] W.-K. Jeong and R. T. Whitaker, *A Fast Iterative Method for Eikonal Equations*, SIAM J. Sci. Comput., 30:5, pp. 2512-2534, 2008.

[25] Kao, C.Y., Osher, S., & Qian, J., *Lax-Friedrichs sweeping scheme for static Hamilton-Jacobi equations*, J. Comput. Phys., 196:1, pp.367–391, 2004.

[26] Kao, C.Y., Osher, S., & Tsai, Y.H., *Fast Sweeping Methods for static Hamilton-Jacobi equations*, SIAM J. Numer. Analy., 42: 2612–2632, 2005.

[27] Kim, S., *An O(N) level set method for eikonal equations*, SIAM J. Sci. Comput., 22, pp. 2178-2193, 2001.

[28] Kimmel, R. & Sethian, J.A., *Fast Marching Methods on Triangulated Domains*, Proc. Nat. Acad. Sci., 95, pp. 8341-8435, 1998.

[29] H.J. Kushner & P.G. Dupuis, *Numerical Methods for Stochastic Control Problems in Continuous Time*, Academic Press, New York, 1992.

[30] F. Li, C.-W. Shu, Y.-T. Zhang and H.-K. Zhao, *A second order DGM based fast sweeping method for Eikonal equations*, Journal of Computational Physics, v.227, pp.8191-8208, 2008.

[31] S. Luo, Y. Yu, H.-K. Zhao, *A new approximation for effective Hamiltonians for homogenization of a class of Hamilton-Jacobi equations*, Multiscale Model. Simul. 9, pp. 711-734, 2011.

[32] A.M. Oberman, R. Takei, and A. Vladimirsky, *Homogenization of metric Hamilton-Jacobi equations*, Multiscale Modeling and Simulation, 8/1, pp. 269-295, 2009.

[33] Pape, U., *Implementation and Efficiency of Moore - Algorithms for the Shortest Path Problem*, Math. Programming, Vol. 7, pp. 212-222, 1974.

[34] L. C. Polymenakos, D. P. Bertsekas, and J. N. Tsitsiklis, *Implementation of Efficient Algorithms for Globally Optimal Trajectories*, IEEE Transactions on Automatic Control, 43(2), pp. 278–283, 1998.

[35] C. Rasch and T. Satzger, *Remarks on the $O(N)$ Implementation of the Fast Marching Method*, IMA J. Numer. Anal. (2009) 29 (3): pp. 806-813.

[36] Rouy, E. & Tourin, A., *A Viscosity Solutions Approach to Shape-From-Shading*, SIAM J. Num. Anal., 29, 3, pp. 867-884, 1992.

[37] J.A. Sethian, *A Fast Marching Level Set Method for Monotonically Advancing Fronts*, Proc. Nat. Acad. Sci., 93, 4, pp. 1591–1595, February 1996.

[38] J.A. Sethian, *Level Set Methods and Fast Marching Methods: Evolving Interfaces in Computational Geometry, Fluid Mechanics, Computer Vision and Materials Sciences*, Cambridge University Press, 1996.

[39] Sethian, J.A., *Fast Marching Methods*, SIAM Review, Vol. 41, No. 2, pp. 199-235, 1999.

[40] J.A. Sethian & A. Vladimirsky, *Fast Methods for the Eikonal and Related Hamilton–Jacobi Equations on Unstructured Meshes*, Proc. Nat. Acad. Sci., 97, 11 (2000), pp. 5699–5703.

[41] J.A. Sethian & A. Vladimirsky, *Ordered Upwind Methods for Static Hamilton-Jacobi Equations*, Proc. Nat. Acad. Sci., 98, 20 (2001), pp. 11069–11074.

[42] J.A. Sethian & A. Vladimirsky, *Ordered Upwind Methods for Static Hamilton-Jacobi Equations: Theory & Algorithms*, SIAM J. on Numerical Analysis 41, 1 (2003), pp. 325-363.

[43] Sethian, J.A. & Vladimirsky, A., *Ordered Upwind Methods for Hybrid Control*, 5th International Workshop, HSCC 2002, Stanford, CA, USA, March 25-27, 2002, Proceedings (LNCS 2289).

[44] Tsai, Y.-H.R., Cheng, L.-T., Osher, S., & Zhao, H.-K., *Fast sweeping algorithms for a class of Hamilton-Jacobi equations*, SIAM J. Numer. Anal., 41:2, pp.659-672, 2003.

[45] J.N. Tsitsiklis, *Efficient algorithms for globally optimal trajectories*, Proceedings, IEEE 33rd Conference on Decision and Control, pp. 1368–1373, Lake Buena Vista, Florida, December 1994.

[46] J.N. Tsitsiklis, *Efficient Algorithms for Globally Optimal Trajectories*, IEEE Tran. Automatic Control, 40 (1995), pp. 1528–1538.

[47] A. Vladimirsky, *Label-setting methods for Multimode Stochastic Shortest Path problems on graphs*, Mathematics of Operations Research 33(4), pp. 821-838, 2008.

[48] O. Weber, Y. Devir, A. Bronstein, M. Bronstein, R. Kimmel *Parallel algorithms for the approximation of distance maps on parametric surfaces*, ACM Transactions on Graphics, 27(4), 2008.

[49] L. Yatziv, A. Bartesaghi, & G. Sapiro, *$O(N)$ implementation of the fast marching algorithm*, J. Comput. Phys. 212 (2006), no. 2, 393-399.

[50] Y.-T. Zhang, S. Chen, F. Li, H.-K. Zhao and C.-W. Shu, *Uniformly accurate discontinuous Galerkin fast sweeping methods for Eikonal equations*, SIAM J. on Sci. Comp., to appear, 2011.

[51] Zhao, H.K., *Fast Sweeping Method for Eikonal Equations*, Math. Comp., 74, pp. 603-627, 2005.